# Electromagnetic coupling and transport in a topological insulator–graphene heterostructure

Daniel A. Bonilla [1,*] Jorge David Castaño-Yepes [1,†] A. Martín-Ruiz,[2,‡] and Enrique Muñoz [1,3,§]

[1]*Facultad de Física, Pontificia Universidad Católica de Chile, Vicuña Mackenna 4860, Santiago, Chile*

[2]*Instituto de Ciencias Nucleares, Universidad Nacional Autónoma de México, 04510 Ciudad de México, México*

[3]*Center for Nanotechnology and Advanced Materials CIEN-UC, Avenida Vicuña Mackenna 4860, Santiago, Chile*

(Received 18 January 2023; revised 16 April 2023; accepted 17 May 2023; published 2 June 2023)

The electromagnetic coupling between heterostructures made of different materials is of great interest, both from the perspective of discovering new phenomena, as well as for its potential applications in novel devices. In this work, we study the electromagnetic coupling of a heterostructure made of a topological insulator (TI) slab and a single graphene layer, where the later presents a diluted concentration of ionized impurities. We explore the topological effects of the magnetoelectric polarizability of the TI, as well as its relative dielectric permittivity on the electrical conductivity in graphene at low but finite temperatures.

DOI: 10.1103/PhysRevB.107.245103

## I. INTRODUCTION

As stated by the great Aristotle more than 2000 years ago in his work *Metaphysics* [1], "*To return to the difficulty which has been stated with respect both to definitions and to numbers, what is the cause of their unity? In the case of all things which have several parts and in which the totality is not, as it were, a mere heap, but the whole is something beside the parts, there is a cause; for even in bodies contact is the cause of unity in some cases, and in others viscosity or some other such quality*." The combination of different materials in the form of heterostructures [2] is our modern quest to search for novel properties that emerge beyond the trivial superposition of those of their individual parts. This search is of great interest not only from a fundamental perspective, since exciting new phenomena may be observed, but also to engineer materials for applications in novel devices. Among the different emerging phenomena in heterostructures, electromagnetic effects are highly relevant for the transmission and storage of energy and information. In this context, the control of electronic transport properties is of fundamental importance.

The discovery of novel materials with nontrivial topological properties [3], such as topological insulators (TIs) [4] and Dirac and Weyl semimetals [5], has introduced a plethora of new phenomenology. In particular, the existence of gapless edge [in two-dimensional (2D) TIs] or surface (in 3D TIs) pseudorelativistic chiral states [6] makes them excellent potential candidates for applications in quantum information technologies and thermoelectrics [7]. In addition, the so-called magnetoelectric polarizability (MEP) [8,9] that locally modifies the constitutive relations between the electromagnetic fields in TIs provides new opportunities to control the magnetoelectric response in such systems. Even though these effects have been extensively studied in individual topological materials, their electromagnetic coupling when integrated into heterostructures remains a vast territory for further exploration [10,11].

In this work, we consider a heterostructure composed of a TI slab and a single graphene layer, as depicted in Fig. 1. We further assume that a diluted concentration of ionized impurities is present in the graphene monolayer. The presence of such charged impurities will induce a local distortion of the charge density of the 2D electron gas, leading to a nontrivial electromagnetic coupling between the TI and the graphene monolayer in the heterostructure. As a probe of this coupling, we further studied the electrical conductivity as a function of temperature, by including the scattering effects with the local electromagnetic field configuration via the Kubo linear response formalism [12–14]. We applied our theoretical results to model the electromagnetic coupling in heterostructures made of different TIs (PbTe, $Bi_2Te_3$, PbSe, PbS, $Bi_2Se_3$, $TlBiSe_2$, $TbPO_4$). Our analytical and numerical results suggest that, among the properties of the TIs, the dielectric permittivity $\epsilon_1$ is the most relevant at tuning the electronic transport in the coupled graphene monolayer. On the other hand, we also observed that the topological effects arising from the presence of the MEP coefficient $\theta$ are comparatively very small even at zero temperature.

## II. ELECTROMAGNETIC RESPONSE OF THE TI

The effective field theory governing the electromagnetic response of topological insulators, independently of the microscopic details, is defined by the action (in SI units) [8]:

$$\mathcal{S} = \int d^4x \left\{ \frac{1}{2}[\epsilon\, \mathbf{E}^2 - (1/\mu)\, \mathbf{B}^2] + \frac{\alpha}{\pi}\sqrt{\frac{\epsilon_0}{\mu_0}}\theta\, \mathbf{E}\cdot\mathbf{B} \right\}, \quad (1)$$

where $\alpha = e^2/(4\pi\epsilon_0\hbar c) \simeq 1/137$ is the fine structure constant, $\epsilon$ and $\mu$ are the permittivity and permeability of the

*dabonilla@uc.cl
†jcastano@uc.cl
‡alberto.martin@nucleares.unam.mx
§munozt@fis.puc.cl

 

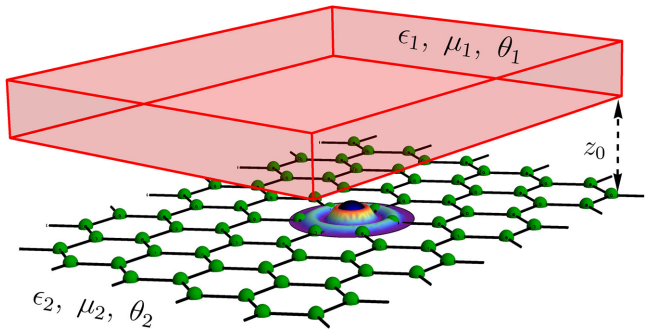


FIG. 1. Pictorial representation of a heterostructure consisting of two materials: a TI slab and a graphene monolayer. The TI slab has material properties of $\epsilon_1$, $\mu_1$, and $\theta_1$, while the graphene monolayer has properties of $\epsilon_2 = 6.9\epsilon_0$, $\mu_2 = \mu_0$, and $\theta_2 = 0$. The two materials are separated by a distance of $z_0$. In the graphene monolayer, there is a diluted concentration of ionized impurities, denoted by $n_{\text{imp}}$, which creates a scattering potential around them.

material, respectively, and $\theta$ is the topological MEP or axion field. The coupling between the gauge field and the free sources is introduced as usual. TR symmetry indicates that $\theta = 0, \pi \pmod{2\pi}$, and hence the $\theta$ term in the action of Eq. (1) has no effect on Maxwell equations in the bulk. The nontrivial topological property, a surface half-integer quantum Hall effect, manifests only when a TR-breaking perturbation is induced on the surface to gap the surface states, thereby converting the material into a full insulator. This can be achieved by introducing magnetic dopants to the surface [15] or by the application of an external static magnetic field [16]. In this situation, $\theta$ is quantized in odd integer values of $\pi$, where the magnitude and sign of the multiple is controlled by the strength and direction of the TR-breaking perturbation.

The field equations arising from the theory of Eq. (1) are those of Maxwell electrodynamics in a medium with the modified constitutive relations [8]

$$\mathbf{D} = \epsilon\mathbf{E} + \alpha\frac{\theta}{\pi}\sqrt{\frac{\epsilon_0}{\mu_0}}\,\mathbf{B}, \quad \mathbf{H} = \frac{1}{\mu}\mathbf{B} - \alpha\frac{\theta}{\pi}\sqrt{\frac{\epsilon_0}{\mu_0}}\,\mathbf{E}. \tag{2}$$

The $\theta$-dependent term in each constitutive equation encodes the most salient feature of this theory: the topological magnetoelectric effect, where an electric field can induce a magnetic polarization and a magnetic field can induce an electric polarization [9].

The general solution to the field equations can be expressed in terms of an indexed Green's function $G_{\mu\nu}$ which satisfies the field equations for a pointlike source and appropriate boundary conditions, namely

$$A^{\mu}(\mathbf{r}) = \int_V G^{\mu}_{\nu}(\mathbf{r},\mathbf{r}')\,J^{\nu}(\mathbf{r}')\,d^3\mathbf{r}', \tag{3}$$

where $\mathbf{r}$ and $\mathbf{r}'$ are the coordinates of the field observation and the source, respectively. Here $A^{\mu} = (\Phi/c, \mathbf{A})$ is the four-potential and $J^{\mu} = (\rho c, \mathbf{J})$ is the four-current density. The exact form of the indexed Green function depends on the geometry configuration of the problem. For example, explicit expressions for the problem of two topologically insulating media separated by a planar interface can be found in Refs. [17,18]. The corresponding expressions for a spherical

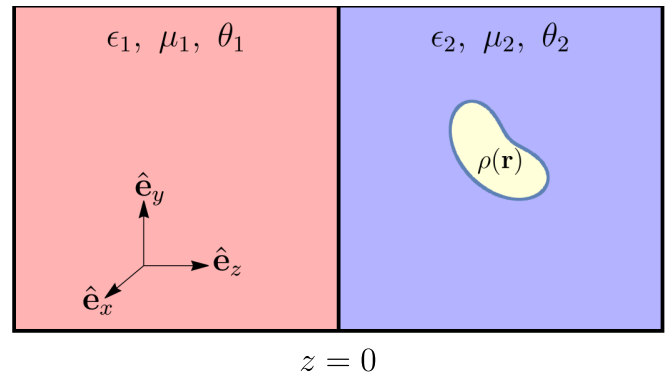


FIG. 2. Charge density $\rho(\mathbf{r})$ near to a planar surface.

interface is reported in Refs. [10,19], and the results for a cylindrial interface have been reported in Ref. [20]. The full expressions are not illuminating at all, so here we just concentrate in the problem at hand, where the source is purely electric, i.e., we take $J^i = 0$.

Let us consider the particular configuration depicted in Fig. 2. The half-space $z < 0$ is occupied by a topological insulator with a dielectric constant $\epsilon_1$, a magnetic permeability $\mu_1$, and MEP $\theta_1$, while the half-space $z > 0$ is occupied by a material (topologically trivial or not) with a dielectric constant $\epsilon_2$, a magnetic permeability $\mu_2$, and MEP $\theta_2$. A charge distribution $\rho(\mathbf{r})$ is placed in the region $z > 0$, as shown in Fig. 2. The electric potential becomes

$$\Phi(\mathbf{r}) = \int \mathcal{G}(\mathbf{r},\mathbf{r}')\,\rho(\mathbf{r}')\,d^3\mathbf{r}', \tag{4}$$

where the corresponding Green function (i.e., the 00 component of the indexed Green's function), for $z > 0$, is

$$\mathcal{G}(\mathbf{r},\mathbf{r}') \equiv G^0_0(\mathbf{r},\mathbf{r}') = \frac{1}{4\pi\epsilon_2}\left(\frac{1}{r_+} + \frac{\kappa}{r_-}\right), \tag{5}$$

with $r_{\pm} = \sqrt{(x-x')^2 + (y-y')^2 + (z \mp z')^2}$ and

$$\kappa \equiv \frac{\epsilon_2 - \epsilon_1 - \Delta}{\epsilon_2 + \epsilon_1 + \Delta}, \quad \Delta \equiv \frac{\mu_1\mu_2}{\mu_1 + \mu_2}\left(\alpha\frac{\theta_1 - \theta_2}{\pi}\sqrt{\frac{\epsilon_0}{\mu_0}}\right)^2. \tag{6}$$

The magnetic response, which is purely topological since the source is electric, is determined by the $0i$ components of the indexed Green's function. One obtains

$$\mathbf{A}(\mathbf{r}) = \int \mathbf{G}(\mathbf{r},\mathbf{r}')\,\rho(\mathbf{r}')\,d^3\mathbf{r}', \tag{7}$$

where the corresponding Green's vector, for $z > 0$, is

$$\mathbf{G}(\mathbf{r},\mathbf{r}') \equiv G^i_0(\mathbf{r},\mathbf{r}')\,\hat{\mathbf{e}}_i = \frac{\mu_1 g}{4\pi}\,\frac{\hat{\mathbf{e}}_z \times \boldsymbol{R}}{R^2}\left(1 - \frac{z + z'}{r_-}\right), \tag{8}$$

with $\boldsymbol{R} = (x - x')\hat{\mathbf{e}}_x + (y - y')\hat{\mathbf{e}}_y$ and

$$g = \alpha\frac{\theta_1 - \theta_2}{\pi}\sqrt{\frac{\epsilon_0}{\mu_0}}\,\frac{\mu_2}{\mu_1 + \mu_2}\,\frac{2}{\epsilon_1 + \epsilon_2 + \Delta}. \tag{9}$$

As expected, in the nontopological limit $\theta_1 \to \theta_2$ we get $\Delta = 0$ and $g = 0$, since the topological magnetoelectricity disappears. Besides, $\kappa \to (\epsilon_2 - \epsilon_1)/(\epsilon_2 + \epsilon_1)$, which is the usual electrostatic result. As a consistency check one can

further verify the image magnetic monopole effect of topological insulators [21]: For a poinlike charge of strength $q$ at $z = z_0$, the electric field can be interpreted in terms of the original charge plus an image charge of strength $\kappa q$ at $-z_0$, and the magnetic field can be interpreted as that of a magnetic monopole of strength $qg$ at $-z_0$.

In the next section we apply the above results to the electronic density distribution that represents the physical configuration depicted in Fig. 1.

## III. ELECTRONIC RESPONSE DUE TO THE IONIZED IMPURITY IN THE GRAPHENE MONOLAYER

In this section, we shall present the effective continuum model, in coordinate space, to account for the electromagnetic effects of a single charged impurity in the monolayer graphene located at a distance $z_0$ from the surface of a planar topological insulator, as shown in Fig. 1. Let us assume that the unperturbed, uniform 2D Dirac fermion gas density in the graphene monolayer is $\Sigma_0 = q\, n_c$, with $n_c = N/A$ the free carrier surface density and $q = \mp e$ the charge for electrons or holes, respectively, depending on the sign of the chemical potential. As a first approximation, we can model this as a uniformly charged plane at a distance $z_0$, with a charge density given by:

$$\rho_{\text{carriers}} = \Sigma_0 \delta(z - z_0). \tag{10}$$

If the ionized impurity has a charge $Q$, and is localized at the point $\mathbf{r}_0$, then it will contribute to the total charge density with a delta distribution $Q\delta(\mathbf{r} - \mathbf{r}_0)$. In response to this charge, the 2D Dirac fermion gas in the graphene monolayer will redistribute itself in order to screen it, leading to a small local deviation from the uniform charge density $\rho(\mathbf{r}) - \rho_{\text{carriers}} \equiv \rho_Y(\mathbf{r})$. After a standard many-body treatment of the 2D electron gas via the random-phase approximation, such screening can be well captured in the static regime via the Thomas-Fermi model [22], that leads to a Yukawa density distribution in coordinate space,

$$\rho_Y(\mathbf{r}) = Q\delta(\mathbf{r} - \mathbf{r}_0) - \frac{Q}{2\pi l_0} \frac{e^{-|\mathbf{r}-\mathbf{r}_0|/l_0}}{|\mathbf{r} - \mathbf{r}_0|} \delta(z - z_0). \tag{11}$$

Here the inverse screening length $l_0^{-1}$ is given by the Thomas-Fermi wave vector $q_{\text{TF}}$, defined by [22]

$$q_{\text{TF}} = \frac{2\pi e^2}{\epsilon_2} D(\epsilon_F), \tag{12}$$

where we have defined the density of states at the Fermi level $\epsilon_F = \hbar v_F k_F$,

$$D(\epsilon_F) = 4 \int \frac{d^2k}{(2\pi)^2} \delta(\hbar v_F k - \epsilon_F) = \frac{2}{\pi} \frac{\epsilon_F}{(\hbar v_F k_F)^2}. \tag{13}$$

Finally, by using the definition of the Fermi wave vector in mono-layer graphene as a function of the free carrier density $n_c$,

$$k_F = \sqrt{\pi n_c}, \tag{14}$$

we obtain from Eq. (12) and Eq. (13) that the Yukawa-screening length is given by

$$l_0^{-1} \equiv q_{\text{TF}} = 4 \frac{e^2}{\epsilon_2} \frac{\sqrt{\pi\, n_c}}{\hbar v_F}. \tag{15}$$

As discussed in the previous section, the presence of this local deviation $\rho_Y(\mathbf{r})$ in the charge density will act as a source to generate an electromagnetic response at the TI, in the form of scalar $\Phi(\mathbf{r})$ and vector potentials $\mathbf{A}(\mathbf{r})$, respectively. These electromagnetic potentials will exist not only at the TI itself but also at the graphene monolayer, thus generating an electromagnetic coupling between the two materials that constitute the heterostructure.

To compute the electromagnetic potentials we use the theory discussed in the previous section. We leave the details of the technical calculations to the Appendix A and we present here only the final results. For definiteness, we evaluate the potentials at $z = z_0$, which is the position of the graphene monolayer as measured from the TI surface (see Fig. 1). We take $\mathbf{r} = \boldsymbol{R} + z_0 \hat{\mathbf{e}}_z$, where $\mathbf{R}$ is a radial vector in the graphene plane measured from the center of the impurity. We first compute the scalar potential $\Phi(\mathbf{r})$, which is given by Eq. (4) with the Green's function given by Eq. (5), with the charge density $\rho_Y(\mathbf{r})$ of Eq. (11). The final result is

$$\Phi(\boldsymbol{R}) = \frac{Q}{4\pi\epsilon_2} \left[ \frac{1}{R} + \frac{\kappa}{\sqrt{R^2 + (2z_0)^2}} - \Lambda_0^{(0)}(R) - \kappa \Lambda_1^{(0)}(R) \right], \tag{16}$$

where $R = |\mathbf{R}|$, and we have defined the functions (for $j = 0, 1$)

$$\Lambda_j^{(\nu)}(R) = \int_0^\infty dk\, \frac{J_\nu(kR)}{\sqrt{1 + (kl_0)^2}}\, e^{-k(2jz_0)}. \tag{17}$$

The mathematical details of the derivation of these functions are presented in the Appendix A. This result can be interpreted as follows: The first term corresponds to the potential due to the original ionized impurity of charge $Q$ at $z_0$, while the second term is due to the image of the ionized impurity, of strength $\kappa Q$ localized at the image point $-z_0$. The third term $\Lambda_0^{(0)}(R)$ corresponds to the electrostatic potential on the monolayer graphene due to the electronic cloud described by the Yukawa term in Eq. (11), and the last term, $\kappa \Lambda_1^{(0)}(R)$, is the image of such electronic cloud. Figure 3 shows the behavior of the scalar potential of Eq. (16) with $z_0 = 3.4$ Å taken as the van der Waals radius of carbon atoms, as a function of $R/a_0$, where $a_0 = 2.46$ Å is the lattice constant of graphene.

We now evaluate the vector potential $\mathbf{A}(\mathbf{r})$, which is given by Eq. (7) with the vector Green's function of Eq. (8) and the charge density $\rho_Y(\mathbf{r})$ of Eq. (11). After some manipulations, fully discussed in the Appendix A, we get

$$\mathbf{A}(\boldsymbol{R}) = \mathbf{A}_{\text{Sch}}(\boldsymbol{R}) - \frac{\mu_2 Q g}{4\pi} \hat{\mathbf{e}}_\phi\, \Lambda_1^{(1)}(R), \tag{18}$$

where the first term $\mathbf{A}_{\text{Sch}}(\mathbf{R})$ is exactly the Schwinger's vector potential of a straight vortex line or Dirac string over the $z$ axis,

$$\mathbf{A}_{\text{Sch}}(\boldsymbol{R}) = \frac{\mu_2 Q g}{4\pi} \frac{\hat{\mathbf{e}}_\phi}{R} \left[ 1 - \frac{2z_0}{\sqrt{R^2 + (2z_0)^2}} \right], \tag{19}$$

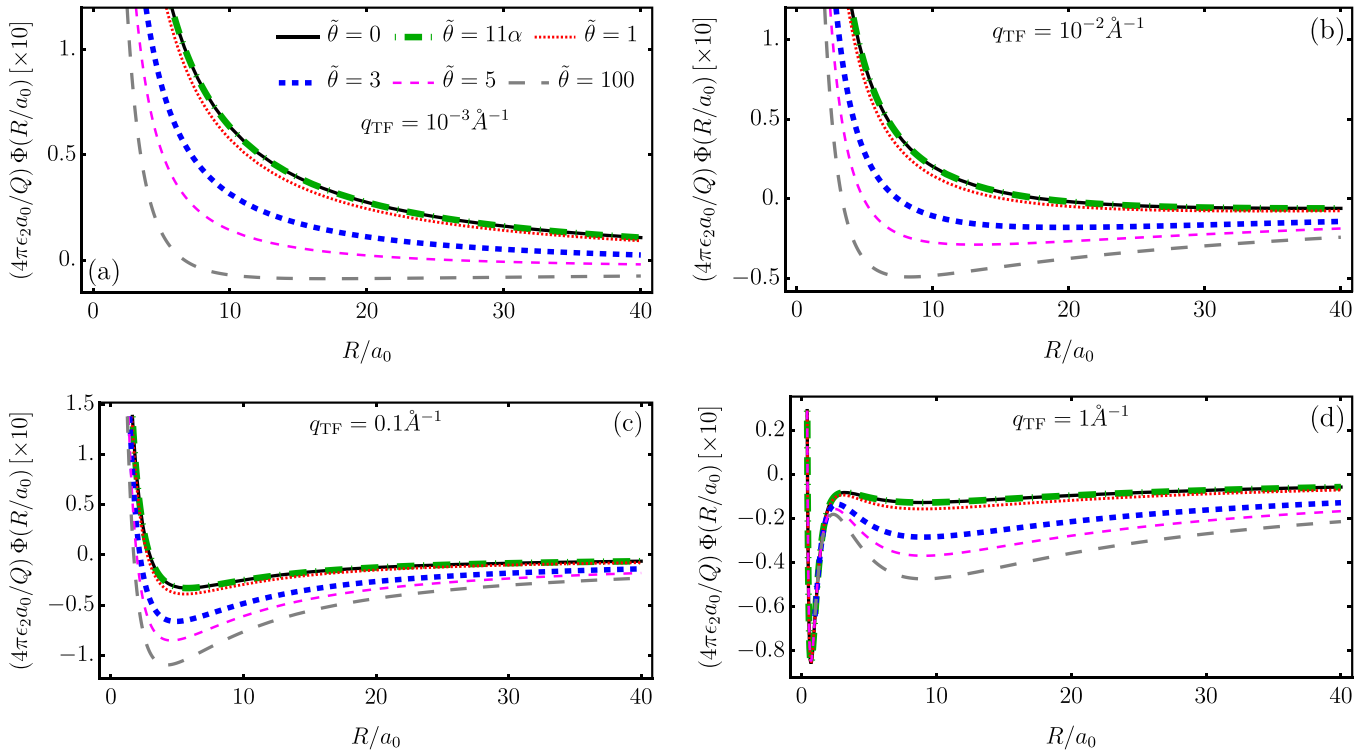


FIG. 3. Scalar potential of Eq. (16) with $z_0 = 3.4$ Å, as a function of $R/a_0$, where $a_0 = 2.46$ Å is the lattice constant of the graphene. The panels are constructed for several values of $q_{\rm TF}$ and $\widetilde{\theta}$, and we fixed $\epsilon_1 = 4\epsilon_0$ and $\epsilon_2 = 6.9\epsilon_0$ corresponding to graphene. For a monovalent cationic impurity with $Q = +e$, the vertical axis is in units of the constant $\frac{Q}{4\pi\epsilon_2 a_0} = 0.847$ (V).

which describes a magnetic monopole of strength $Qg$ at the image point $-z_0$. The second term, proportional to $\hat{\mathbf{e}}_\phi\,\Lambda_1^{(1)}(R)$, corresponds to the magnetic response due to the electronic screening cloud described by the Yukawa term.

To take into account the effects of mobile charge in the graphene layer, we must consider the total 4-potential given by:

$$A_T^\mu = A_\theta^\mu + A^\mu_{\rm carriers}, \tag{20}$$

where $A_\theta^\mu$ is given by Eqs. (16) and (18), so that

$$A_\theta^\mu = (\Phi(R), \mathbf{A}(\mathbf{R})), \tag{21}$$

and $A^\mu_{\rm carriers}$ is the contribution of the free mobile charge distributed in the graphene layer, described by the uniform two-dimensional distribution Eq. (10), which is ultimately responsible for the electrical conduction process.

From the above, it is straightforward to show that:

$$\Phi_{\rm carriers}(z) = \Phi(z_0) + \frac{\Sigma_0}{2\epsilon_2}(z - z_0), \tag{22}$$

where, without loss of generality, the ground can be set at the graphene plane $z = z_0$, so that $\Phi(z_0) = 0$.

On the other hand, due to the symmetry of the problem, the induced magnetic image charge will produce a constant and static magnetic field along the $\hat{\mathbf{z}}$ direction. To ensure gauge invariance of our theory, we model this field as

$$\mathbf{A}_{\rm carriers}(\mathbf{R}) = \frac{R B_0}{2}\hat{\mathbf{e}}_\phi, \tag{23}$$

where $B_0 = -\frac{1}{2}\mu_2 g \Sigma_0$.

Thus, we have

$$A^\mu_{\rm carriers} = \left(0, \frac{R B_0}{2}\,\hat{\mathbf{e}}_\phi\right). \tag{24}$$

Applying our previous explicit results for the electromagnetic response of the TI, we will study the electrical conductivity in the coupled graphene monolayer. For this purpose, we first need to analyze the scattering mechanism experienced by the massless Dirac fermions in the graphene monolayer, due to the presence of the local electromagnetic fields resulting from this coupling, which is the subject of the next section.

## IV. SCATTERING ANALYSIS AND PHASE SHIFT

In this section, we shall analyze the scattering mechanism experienced by massless Dirac fermions in the graphene monolayer coupled to the TI slab, as shown in the heterostructure depicted by Fig. 1. As discussed in the previous section, the electromagnetic coupling between the TI and the graphene monolayer in the presence of ionized impurities, will generate a local electromagnetic field characterized by the scalar and vector potential $\Phi(\mathbf{R})$ and $\mathbf{A}(\mathbf{R})$, as given by Eq. (16) and Eq. (18), respectively. Therefore, the dynamics of the charge carriers in the 2D graphene monolayer is determined by the effective Hamiltonian (with the minimal coupling prescription):

$$\hat{H}^\xi = \xi v_F \boldsymbol{\sigma}\cdot[\hat{\mathbf{p}} - q\mathbf{A}(\mathbf{R})] + q\Phi(\mathbf{R})\hat{I}, \tag{25}$$

where as before, $\mathbf{R}$ represents a 2D vector laying in the graphene plane, $\xi = \pm 1$ is the valley index for each of the Dirac $K_\pm$ points, $v_F$ is the Fermi velocity, and $q = \mp e$ is the

fermion's electric charge (electrons or holes depending on the sign of the chemical potential).

As seen in Eq. (16) and Eq. (18), the electromagnetic fields generated by the coupling decay at long distances with respect to the position of the impurity. Therefore, we can apply the standard assumptions in scattering theory, i.e., that incident fermions far from the impurity are described by asymptotically free particle states, with momentum $\mathbf{k}$, and band index $\lambda = \pm 1$. In polar coordinates, those are given by the bispinors

$$\langle \mathbf{R}|\Phi_{\mathbf{k},\lambda}\rangle = \Phi_{\mathbf{k},\lambda}(\mathbf{R}) = \frac{1}{\sqrt{2}}\begin{bmatrix}1\\ \lambda\end{bmatrix} e^{i\mathbf{k}\cdot\mathbf{R}} = \frac{1}{\sqrt{2}}\begin{bmatrix}1\\ \lambda\end{bmatrix} e^{ikR\cos\phi}, \tag{26}$$

with energy

$$\mathcal{E}_{\mathbf{k}}^{(\lambda,\xi)} = \lambda\xi\hbar v_F|\mathbf{k}|. \tag{27}$$

Now, it is convenient to use the identity

$$e^{ikR\cos\phi} = \sum_{m=-\infty}^{\infty} i^m e^{im\phi} J_m(kR), \tag{28}$$

in order to expand the incident spinor into angular momentum channels $m \in \mathbb{Z}$,

$$\Phi_{\mathbf{k},\lambda}(\mathbf{R}) = \frac{1}{\sqrt{2}}\sum_{m=-\infty}^{\infty} i^m \begin{bmatrix} J_m(kR)e^{im\phi} \\ i\lambda J_{m+1}(kR)e^{i(m+1)\phi}\end{bmatrix}. \tag{29}$$

Due to the azymuthal symmetry of the system, we can also expand the angular dependence of the eigenspinor of the full Hamiltonian into angular momentum channels

$$\begin{aligned}\langle \mathbf{R}|\Psi_{\mathbf{k},\lambda}\rangle &= \Psi_{\mathbf{k},\lambda}(\mathbf{R}) \\ &= \frac{1}{\sqrt{2}}\sum_{m=-\infty}^{\infty} i^m \begin{bmatrix} f_m(kR)e^{im\phi} \\ i\lambda g_m(kR)e^{i(m+1)\phi}\end{bmatrix},\end{aligned} \tag{30}$$

where the radial dependence is implicit in the functions $f_m(kR)$ and $g_m(kR)$, that are yet to be determined, as we show in Appendix B. From the Lippmann-Schwinger formalism in terms of the retarded and advanced Green's functions, the final asymptotic states can also be decomposed into angular-momentum channels. To do so, we consider that the electromagnetic potential possesses a compact support, i.e., it decays with a characteristic distance $a$, so that for $R > a$ the interaction potential becomes negligible. Then, the eigenspinors can be found from the following self-consistent integral equations: For $R < a$

$$\begin{aligned}\begin{bmatrix} f_m(R)\\ g_m(R)\end{bmatrix} = \begin{bmatrix} J_m(kR)\\ J_{m+1}(kR)\end{bmatrix} &- \frac{\lambda\xi i\pi k}{2\hbar v_F}\int_0^R dR'R' \begin{bmatrix} J_m(kR')H_m^{(1)}(kR) & J_{m+1}(kR')H_m^{(1)}(kR)\\ J_m(kR')H_{m+1}^{(1)}(kR) & J_{m+1}(kR')H_{m+1}^{(1)}(kR)\end{bmatrix}\begin{bmatrix} e\Phi(R') & -\lambda\xi q v_F A(R')\\ -\lambda\xi q v_F A(R') & e\Phi(R')\end{bmatrix}\begin{bmatrix} f_m(R')\\ g_m(R')\end{bmatrix} \\ &- \frac{\lambda\xi i\pi k}{2\hbar v_F}\int_R^a dR'R' \begin{bmatrix} J_m(kR)H_m^{(1)}(kR') & J_{m+1}(kR)H_m^{(1)}(kR')\\ J_m(kR)H_{m+1}^{(1)}(kR') & J_{m+1}(kR)H_{m+1}^{(1)}(kR')\end{bmatrix}\begin{bmatrix} e\Phi(R') & -\lambda\xi q v_F A(R')\\ -\lambda\xi q v_F A(R') & e\Phi(R')\end{bmatrix}\begin{bmatrix} f_m(R')\\ g_m(R')\end{bmatrix},\end{aligned} \tag{31}$$

and for $R > a$ we have

$$\begin{bmatrix} f_m(R)\\ g_m(R)\end{bmatrix} = \begin{bmatrix} J_m(kR)\\ J_{m+1}(kR)\end{bmatrix} - \frac{\lambda\xi i\pi k}{2\hbar v_F}\int_0^a dR'R' \begin{bmatrix} J_m(kR')H_m^{(1)}(kR) & J_{m+1}(kR')H_m^{(1)}(kR)\\ J_m(kR')H_{m+1}^{(1)}(kR) & J_{m+1}(kR')H_{m+1}^{(1)}(kR)\end{bmatrix}\begin{bmatrix} e\Phi(R') & -\lambda\xi e v_F A(R')\\ -\lambda\xi e v_F A(R') & e\Phi(R')\end{bmatrix}\begin{bmatrix} f_m(R')\\ g_m(R')\end{bmatrix}, \tag{32}$$

which we label as *internal* and *external* solutions, respectively.

From the above states, the so-called phase shift $\delta_m$ is easily computed from the *external* solution (because it carries the scattering information) as

$$e^{i\delta_m(k)}\sin\delta_m(k) = -\frac{\lambda\xi\pi k}{4\hbar v_F}\int_0^a dR'R' \begin{bmatrix} J_m(kR') & J_{m+1}(kR')\end{bmatrix}\begin{bmatrix} q\Phi(R') & -\lambda\xi q v_F A(R')\\ -\lambda\xi q v_F A(R') & q\Phi(R')\end{bmatrix}\begin{bmatrix} f_m(R')\\ g_m(R')\end{bmatrix}, \tag{33}$$

so that the spinor $[f_m(R'), g_m(R')]^T$ is given by the internal solution (because it is the region that produced the scattering).

## V. RELAXATION TIME AND ELECTRICAL CONDUCTIVITY

In order to compute the microscopic transport coefficients, we define the quantum operators, related to the particle, energy, and heat currents, respectively:

$$\hat{\mathbf{j}} = \sum_{\mathbf{p}\sigma}\mathbf{v}_{\mathbf{p}}\hat{n}_{\mathbf{p}\sigma}, \tag{34}$$

$$\hat{\mathbf{j}}_E = \sum_{\mathbf{p}\sigma}\mathbf{v}_{\mathbf{p}}\mathcal{E}_{\mathbf{p}\sigma}\hat{n}_{\mathbf{p}\sigma}, \tag{35}$$

$$\hat{\mathbf{j}}_Q = \sum_{\mathbf{p}\sigma}\mathbf{v}_{\mathbf{p}}(\mathcal{E}_{\mathbf{p}\sigma} - \mu)\hat{n}_{\mathbf{p}\sigma}, \tag{36}$$

where for a particle with momentum $\mathbf{p}$ and spin $\sigma$, we identify $\mathbf{v}_{\mathbf{p}}$ as the group velocity, $\hat{n}_{\mathbf{p}\sigma}$ as the particle number density operator, $\mathcal{E}_{\mathbf{p}\sigma}$ as the energy, and $\mu$ as the chemical potential of the system. The corresponding macroscopic observed currents are given by the ensemble average of the above operators, i.e.,

$$\mathbf{J} = \langle\hat{\mathbf{j}}\rangle, \tag{37a}$$

$$\mathbf{J}_E = \langle\hat{\mathbf{j}}_E\rangle, \tag{37b}$$

$$\mathbf{J}_Q = \langle\hat{\mathbf{j}}_Q\rangle. \tag{37c}$$

As is shown in Appendix C 1, the currents are coupled to the temperature and electrochemical potential gradients

through the so-called Onsager's coefficients, which in tensor notation take the form [23]:

$$\mathbf{J} = -\frac{1}{T}\overleftrightarrow{\mathbf{L}}^{(11)}\cdot\nabla(\mu+eV) + \overleftrightarrow{\mathbf{L}}^{(12)}\cdot\nabla\left(\frac{1}{T}\right), \quad (38a)$$

$$\mathbf{J}_Q = -\frac{1}{T}\overleftrightarrow{\mathbf{L}}^{(21)}\cdot\nabla(\mu+eV) + \overleftrightarrow{\mathbf{L}}^{(22)}\cdot\nabla\left(\frac{1}{T}\right). \quad (38b)$$

Here $T$ is the system's temperature and $V$ the external bias voltage that triggers the electric current. Then, the electrical conductivity tensor is found by imposing the isothermal condition $\nabla T = 0$

$$\overleftrightarrow{\boldsymbol{\sigma}} = \frac{e^2}{T}\overleftrightarrow{\mathbf{L}}^{(11)}, \quad (39)$$

the thermal conductivity tensor is defined by $\mathbf{J} = 0$,

$$\overleftrightarrow{\boldsymbol{\kappa}} = \frac{1}{T^2}\left(\overleftrightarrow{\mathbf{L}}^{(22)} - \overleftrightarrow{\mathbf{L}}^{(21)}\cdot\left[\overleftrightarrow{\mathbf{L}}^{(11)}\right]^{-1}\cdot\overleftrightarrow{\mathbf{L}}^{(12)}\right), \quad (40)$$

and the Seebeck coefficient or thermopower is given by

$$S = \frac{1}{eT}\left[\overleftrightarrow{\mathbf{L}}^{(11)}\right]^{-1}\cdot\overleftrightarrow{\mathbf{L}}^{(12)}. \quad (41)$$

The connection of the Onsager's coefficients with the microscopic dynamical variables is given by the Kubo's linear response theory. In the Appendix C 2 we show that for the particle current operator

$$\hat{\mathbf{j}}^{(\xi)}(\mathbf{R}) = \xi v_F|\mathbf{R}\rangle\boldsymbol{\sigma}\langle\mathbf{R}|, \quad (42)$$

and the heat current operator

$$\hat{\mathbf{j}}_Q^{(\xi)}(\mathbf{R}) = \xi v_F(\hat{H}^\xi - \mu)|\mathbf{R}\rangle\boldsymbol{\sigma}\langle\mathbf{R}|, \quad (43)$$

given the thermal equilibrium density operator

$$\hat{\rho}_0 = \frac{\exp[-\beta(\hat{H}^\xi-\mu)]}{\mathrm{Tr}[\exp[-\beta(\hat{H}^\xi-\mu)]]}, \quad (44)$$

the Onsager's coefficients take the form [24]

$$L_{\alpha\beta}^{(11)} = -T\int_0^\infty dt\, e^{-st}\int_0^\beta d\beta'\,\mathrm{Tr}[\hat{\rho}_0\hat{j}_\alpha(-t-i\hbar\beta')\hat{j}_\beta], \quad (45a)$$

$$L_{\alpha\beta}^{(12)} = L_{\alpha\beta}^{(21)} = -T\int_0^\infty dt\, e^{-st}\int_0^\beta d\beta'\,\mathrm{Tr}[\hat{\rho}_0\hat{j}_{Q\alpha}(-t-i\hbar\beta')\hat{j}_\beta], \quad (45b)$$

$$L_{\alpha\beta}^{(22)} = -T\int_0^\infty dt\, e^{-st}\int_0^\beta d\beta'\,\mathrm{Tr}[\hat{\rho}_0\hat{j}_{Q\alpha}(-t-i\hbar\beta')\hat{j}_{Q\beta}]. \quad (45c)$$

These expressions are reduced to a more explicit form by introducing the spectral density function [12]

$$\boldsymbol{\mathcal{A}}^\xi(\mathbf{R},\mathbf{R}';E) = 2\pi\sum_\lambda\int\frac{d^2k}{(2\pi)^2}\Psi_{\lambda,\mathbf{k}}(\mathbf{R})\otimes\Psi_{\lambda,\mathbf{k}}^\dagger(\mathbf{R}')\delta\left(E-\mathcal{E}_{\mathbf{k}}^{(\lambda,\xi)}\right), \quad (46)$$


FIG. 4. The Bethe-Salpeter integral equation for the vertex function $\boldsymbol{\Gamma}_{\mathrm{RA}}(\mathbf{k})$.

and its relationship with the retarded and advanced Green's functions:

$$\mathcal{A}^{(\lambda,\xi)}(k;E) = i\left[\left\langle G_R^{(\lambda,\xi)}(k;E)\right\rangle - \left\langle G_A^{(\lambda,\xi)}(k;E)\right\rangle\right], \quad (47)$$

so that, for instance, the coefficient $L_{\alpha\beta}^{(11)}$ takes the form:

$$L_{\alpha\beta}^{(11)}(T) = \delta_{\alpha\beta}4\pi\left[\frac{\hbar v_F^2 T}{(2\pi)^3}\right]\int_{-\infty}^\infty dE\left[-\frac{\partial f_0(E)}{\partial E}\right]\times\int_0^\infty dk\left\langle G_R^{(\lambda,\xi)}(k;E)\right\rangle\left\langle G_A^{(\lambda,\xi)}(k;E)\right\rangle\frac{\mathbf{k}\cdot\mathbf{k}}{k}. \quad (48)$$

where $f_0(E,T) = \{1+\exp[(E-\mu)/kT]\}^{-1}$ is the Fermi-Dirac distribution.

By following Ref. [12] (see Appendix C 3 for details) it is possible to include vertex corrections to the formalism. For that purpose, one of the $\mathbf{k}$ factors is replaced by the vertex correction $\boldsymbol{\Gamma}_{\mathrm{RA}}(\mathbf{k},E)$, that satisfies the *Bethe-Salpeter equation* (see Fig. 4):

$$\boldsymbol{\Gamma}_{\mathrm{RA}}(\mathbf{k},E) = \mathbf{k} + n_{\mathrm{imp}}\int\frac{d^2k'}{(2\pi)^2}\left\langle G_R^{(\lambda,\xi)}(\mathbf{k}')\right\rangle\left\langle G_A^{(\lambda,\xi)}(\mathbf{k}')\right\rangle\times\left|\hat{T}_{\mathbf{k}'\mathbf{k}}^{(\lambda,\xi)}\right|^2\boldsymbol{\Gamma}_{\mathrm{RA}}(\mathbf{k}',E), \quad (49)$$

where $\hat{T}_{\mathbf{k}'\mathbf{k}}^{(\lambda,\xi)}$ is the $T$-matrix operator.

Therefore, when vertex corrections are incorporated then Eq. (48) (as well as the other coefficients) is modified as

$$L_{\alpha\beta}^{(11)}(T) = \delta_{\alpha\beta}\frac{\hbar v_F^2 T}{2\pi^2}\int_{-\infty}^\infty dE\left[-\frac{\partial f_0(E)}{\partial E}\right]\times\int_0^\infty dk\left\langle G_R^{(\lambda,\xi)}(\mathbf{k})\right\rangle\left\langle G_A^{(\lambda,\xi)}(\mathbf{k})\right\rangle\frac{\mathbf{k}\cdot\boldsymbol{\Gamma}_{\mathrm{RA}}(\mathbf{k},E)}{k}, \quad (50)$$

$$L_{\alpha\beta}^{(12)}(T) = \delta_{\alpha\beta}\frac{\hbar v_F^2 T}{2\pi^2}\int_{-\infty}^\infty dE\left[-\frac{\partial f_0(E)}{\partial E}\right](E-\mu)\times\int_0^\infty dk\left\langle G_R^{(\lambda,\xi)}(\mathbf{k})\right\rangle\left\langle G_A^{(\lambda,\xi)}(\mathbf{k})\right\rangle\frac{\mathbf{k}\cdot\boldsymbol{\Gamma}_{\mathrm{RA}}(\mathbf{k},E)}{k}, \quad (51)$$

and

$$L_{\alpha\beta}^{(22)}(T) = \delta_{\alpha\beta}\frac{\hbar v_F^2 T}{2\pi^2}\int_{-\infty}^\infty dE\left[-\frac{\partial f_0(E)}{\partial E}\right](E-\mu)^2\times\int_0^\infty dk\left\langle G_R^{(\lambda,\xi)}(\mathbf{k})\right\rangle\left\langle G_A^{(\lambda,\xi)}(\mathbf{k})\right\rangle\frac{\mathbf{k}\cdot\boldsymbol{\Gamma}_{\mathrm{RA}}(\mathbf{k},E)}{k}. \quad (52)$$

Following Ref. [12], as is shown in Appendix C 3, by considering the general form $\boldsymbol{\Gamma}_{\mathrm{RA}}(\mathbf{k},E) = \gamma(\mathbf{k},E)\mathbf{k}$, the re-

laxation time can be introduced with the relation

$$\gamma(k_F) = \frac{\tau_1(k_F)}{\tau_1(k_F) - \tau(k_F)}, \tag{53}$$

where we defined (for $\cos\phi' = \mathbf{k}\cdot\mathbf{k}'/k^2$)

$$\frac{1}{\tau_1(k_F)} = \frac{2\pi n_{\rm imp}}{\hbar}\int \frac{d^2k'}{(2\pi)^2}\left|T^{(\lambda,\xi)}_{\mathbf{k}'\mathbf{k}}\right|^2 \cos\phi'\ \delta(\hbar v_F k_F - \hbar v_F k'). \tag{54}$$

so that, by following Ref. [12] the total *transport relaxation time* is defined by

$$\frac{1}{\tau_{\rm tr}(k_F)} = \frac{1}{\tau(k_F)} - \frac{1}{\tau_1(k_F)} = \frac{2\pi n_{\rm imp}}{\hbar} \times \int \frac{d^2k'}{(2\pi)^2}\delta(\hbar v_F k_F - \hbar v_F k')\left|T^{(\lambda,\xi)}_{\mathbf{k}'\mathbf{k}}\right|^2(1-\cos\phi'), \tag{55}$$

which can be expressed in terms of the scattering phase shifts $\delta_m(k)$ of Eq. (33) as

$$\frac{1}{\tau_{\rm tr}(k_F)} = \frac{2n_{\rm imp}v_F}{k_F}\sum_{m=-\infty}^{\infty}\sin^2\left[\delta_m(k_F) - \delta_{m-1}(k_F)\right]. \tag{56}$$

With all these ingredients, as is computed in Appendices C 4 and C 5, the electrical conductivity is

$$\sigma_{xx}(T) = 4\left(\frac{e^2}{h}\right)k_F v_F\,\tau_{\rm tr}(k_F) \times\left[1 + 2\frac{k_B T}{v_F\hbar k_F}\ln\left(1+\exp\left[-\frac{\hbar k_F v_F}{k_B T}\right]\right)\right], \tag{57}$$

and the thermal conductivity and the Seebeck coefficient are, respectively, given by

$$\kappa_{\alpha\alpha}(T) = -\frac{2\hbar^2}{\pi k_B T^2}\left(\frac{k_B T}{\hbar}\right)^4\tau_{\rm tr}(k_F) \times\sum_{\lambda,\xi=\pm1}\left[3\,{\rm Li}_3\left(-e^{\frac{\lambda\xi\hbar v_F k_F}{k_B T}}\right) - 2\frac{\left[{\rm Li}_2\left(-e^{\frac{\lambda\xi\hbar v_F k_F}{k_B T}}\right)\right]^2}{\ln\left(1+e^{\frac{\lambda\xi\hbar v_F k_F}{k_B T}}\right)}\right]. \tag{58}$$

$$S(T) = \frac{1}{eT}\sum_{\lambda,\xi}\frac{L^{(12)(\lambda,\xi)}_{\alpha\alpha}(T)}{L^{(11)(\lambda,\xi)}_{\alpha\alpha}(T)} = -\frac{k_B}{e}\sum_{\lambda=\pm1}\sum_{\xi=\pm1}\left(\frac{2\lambda\xi\,{\rm Li}_2\left(-e^{\frac{\lambda\xi\hbar v_F k_F}{k_B T}}\right)}{\ln\left(1+e^{\frac{\lambda\xi\hbar v_F k_F}{k_B T}}\right)} + \frac{\hbar v_F k_F}{k_B T}\right). \tag{59}$$

## VI. RESULTS AND DISCUSSION

In the following, we set the Fermi velocity in graphene as $v_F = 10^{16}$ Å s$^{-1}$, the chiral and band indexes as $\xi = 1$, and $\lambda = 1$, and the distance between the TI surface and the graphene monolayer as $z_0 = 3.4$ Å, corresponding to the van der Waals radius of the carbon atoms. As a function of the free carrier density in graphene $n_c$, we obtain the Fermi $k_F$, and the Thomas-Fermi $q_{\rm TF}$ wave vectors as defined by Eq. (14) and Eq. (15), respectively, and the corresponding Yukawa screening length $l_0 = q_{\rm TF}^{-1}$.

Moreover, for a monovalent ionic impurity the charge $Q = +e$, all the magnetic permeabilities are fixed to unity, and the relative dielectric permittivity $\epsilon_2$ is taken as 6.9, corresponding to graphene for which we assume $\theta_2 = 0$.

TABLE I. Material constants for $TlBiSe_2$ and $TbPO_4$.

| Material | $\epsilon_r$ | $\tilde{\theta}$ | Ref. |
|---|---|---|---|
| $TlBiSe_2$ | 4 | $11\alpha$ | [25] |
| $TbPO_4$ | 3.5 | 0.22 | [26] |

### A. The role of the MEP $\theta_1$

To test the impact of the topological component, represented by the MEP parameter $\theta_1$, on the electromagnetic coupling between the TI and the massless Dirac fermions in graphene, we compute the electrical conductivity from Eq. (57) for two different materials: $TlBiSe_2$, and $TbPO_4$. Those materials are characterized by the parameters displayed in Table I, where $\tilde{\theta} \equiv \alpha\theta_1/\pi$.

Figure 5 shows the electrical conductivity in the graphene monolayer (with a carrier density $n_c = 10^{12}$ m$^{-2}$) computed from Eq. (57) when the TI slab is made of $TlBiSe_2$. To elucidate the impact of the topological MEP terms, we implemented the cases $\tilde{\theta} = 0$ and $\tilde{\theta} = 11\alpha$, as Table I indicates. As can be noticed, the topological effects are negligible even for low temperatures, where the residual conductivity is modified just by a factor ∼0.01%.

When the carrier density is increased to $n_c = 10^{17}$ m$^{-2}$, the picture does not change much: As is depicted in Fig. 6, the effect of the topological MEP term remains small. Nevertheless, the electrical conductivity remains essentially constant for temperatures up to 300 K, and therefore the (small) effects of the topological MEP terms remain present at room temperature. The same behavior is found for $TbPO_4$, i.e., the effects

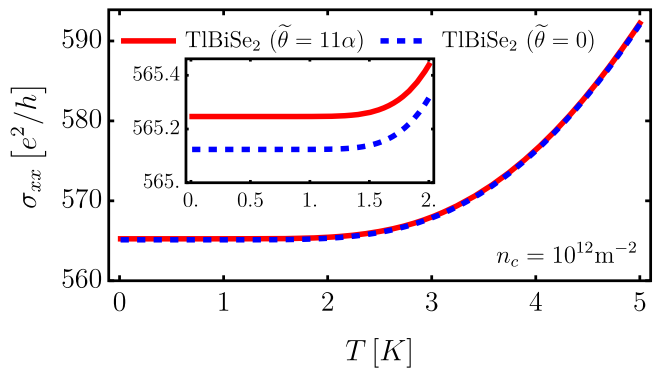


FIG. 5. Electrical conductivity in the graphene monolayer $\sigma_{xx}$ as a function of temperature. Each curve corresponds to a $TlBiSe_2$ TI slab, with and without the contribution from the MEP term. The inset is included to appreciate the small deviations at low-temperatures. The impurity concentration is taken as $n_{\rm imp} = 10^{12}$ m$^{-2}$.

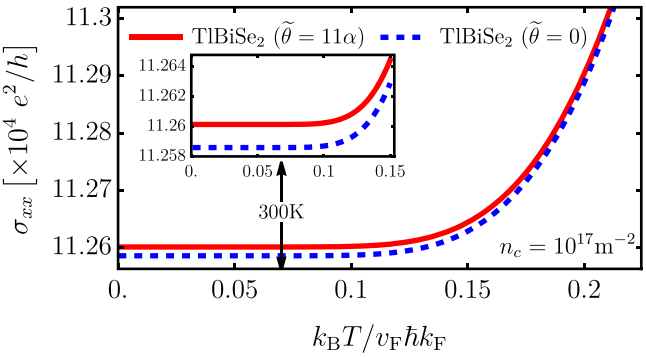


FIG. 6. Electrical conductivity in the graphene monolayer $\sigma_{xx}$ as a function of the dimensionless temperature $k_BT/v_F\hbar k_F$. Each curve corresponds to a slab made of $TlBiSe_2$ with and without the contribution from the MEP. The inset is included to appreciate the small deviations at low temperatures, and the arrows indicate the absolute temperature $T = 300$ K. The impurity concentration is taken as $n_{\mathrm{imp}} = 10^{17}$ m$^{-2}$.

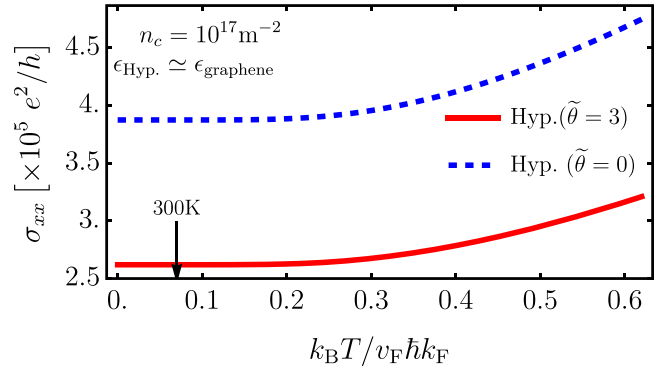


FIG. 7. Graphene's electrical conductivity $\sigma_{xx}$ as a function of the dimensionless temperature $k_BT/v_F\hbar k_F$. Each curve corresponds to a slab made of an hypothetical TI material with $\epsilon_1 = \epsilon_{\mathrm{Hyp.}} \simeq \epsilon_{\mathrm{graphene}}$. The arrow indicates the absolute temperature $T = 300$ K. The impurity concentration is taken as $n_{\mathrm{imp}} = 10^{12}$ m$^{-2}$.

of the topological MEP $\theta$ terms on the electrical conductivity remain very small, on the order of 0.1%.

In order to understand the effects of the MEP terms, let us analyze Fig. 3, where we represent the dimensionless scalar potential in units of the constant $\frac{Q}{4\pi\epsilon_2 a_0} = 0.847$ V, where for definiteness we assume $a_0 = 2.46$ Å for the graphene lattice constant, $\epsilon_2 = 6.9\epsilon_0$, and a monovalent cationic impurity with $Q = +e$. Here, the panels are constructed for several values of the Thomas-Fermi wave vector $q_{\mathrm{TF}}$ and the MEP $\widetilde{\theta}$. As can be appreciated, the topological effects are sensitive to the value of $q_{\mathrm{TF}}$, which implies that the integration regions for the Eqs. (31)–(33) need to be carefully fixed for each window of parameters. For instance, Fig. 3 implies that the scalar potential is negligible for $\rho \gtrsim 40a_0$. To have an insight into these results in terms of the intrinsic graphene parameters, the Thomas-Fermi wave vector $q_{\mathrm{TF}}$ can be calculated as a function of the corresponding free carrier density $n_c$. Therefore, by following Eq. (15) we choose the four cases

$$n_c^{(\mathrm{a})} = 3.2\times 10^{13}\ \mathrm{m}^{-2}, \quad n_c^{(\mathrm{b})} = 3.2\times 10^{15}\ \mathrm{m}^{-2}$$
$$n_c^{(\mathrm{c})} = 3.2\times 10^{17}\ \mathrm{m}^{-2}, \quad n_c^{(\mathrm{d})} = 3.2\times 10^{19}\ \mathrm{m}^{-2}, \qquad (60)$$

where the superindexes (a)–(d) correspond to the panels in Figs. 3(a)–3(d), respectively. Note that despite the hierarchy and deviations between the magnitude of the potential as a function of $\tilde{\theta}$ remain, for higher carrier densities the topological effects contribute to a slower decay of the potential, that then sustains finite values at longer distances [see Fig. 3(d)]. Moreover, as seen in the same figure the potential develops two minima, that can be attributed to the contribution arising from the MEP topological term. The presence of such minima may suggest the possibility for the emergence of bounded states, but those are only possible in a Coulomb potential for gapped graphene, where the Dirac fermions acquire a finite effective mass proportional to the gap [27], while in our system the carriers remain gapless and hence massless. Moreover, as reported in the literature, first-principles calculations that go beyond the linear Dirac approximation [28] estimate that the binding energies for electrons to ionized cationic impurities in graphene, such as Li or Na, are close to 1 eV [28]. However, even for the more extreme cases calculated and represented in Fig. 3, the depth of the minima are on the order of $|e\Phi| \leqslant 1.0\times 10^{-1}\times\frac{eQ}{4\pi\epsilon_2 a_0} \sim 0.085$ eV, which is too shallow to allow for such bound state, and hence this possibility is ruled out from our physical scenario. The emergence of the minima implies that the topological terms are comparatively less screened by the free carriers than the trivial ones. Nevertheless, it is important to point out that the state-of-the-art estimations for the value of $\tilde{\theta}$ suggest that it is small (see Table I). Hence, as Fig. 3 shows, the topological contribution to the electromagnetic coupling can be neglected unless the TI material satisfies $\theta > 137\pi$. The later scenario is shown Fig. 7, where we plot the electrical conductivity for a TI hypothetical material with $\widetilde{\theta} = 3$ and a dielectric constant close to graphene. In this particular configuration, even at room temperature the topological effects are significant, leading to a strong suppression of the electrical conductivity in the graphene monolayer. This effect can be attributed to the topologically nontrivial magnetoelectric coupling, which becomes appreciable for large values of $\theta$ ($\kappa \gg g$ for small values of $\theta$). This magnetoelectric coupling affects the carrier dynamics, resulting in additional scattering processes. Additionally, as in the case of realistic MEP's values, if the graphene carrier density is increased, the topological effects can be differentiated from the trivial ones up to room temperature. In contrast, for low $n_c$, the topological MEP terms induce appreciable deviations only at low temperatures, as seen by comparing Figs. 5 and 6 and Figs. 8 and 9, respectively.

### B. The role of $\epsilon_1$

An essential characteristic of the scalar potential of Eq. (16) is its dependence on the dielectric constant through the $\kappa$ factor in Eq. (6). In particular, by ignoring the topological parameters $\theta$, the combination $(\epsilon_2 - \epsilon_1)/(\epsilon_2 + \epsilon_1)$ can be understood as an effective image charge located at the slab. Therefore, we present the change in the conductivity as a function of this image charge when the relative permittivity $\epsilon_2$ is fixed as the graphene one.

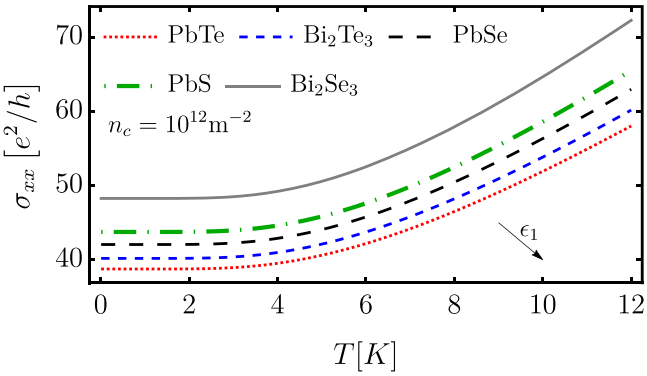


FIG. 8. Electrical conductivity of graphene $\sigma_{xx}$ as a function of temperature for $n_c = 10^{12}$ m$^{-2}$. Each curve corresponds to different TI materials for the slab. The relative permittivity $\epsilon_1$ of each TI is shown in Table II. The arrow points the direction in which $\epsilon_1$ increases. The impurity concentration is taken as $n_{\mathrm{imp}} = 10^{12}$ m$^{-2}$.

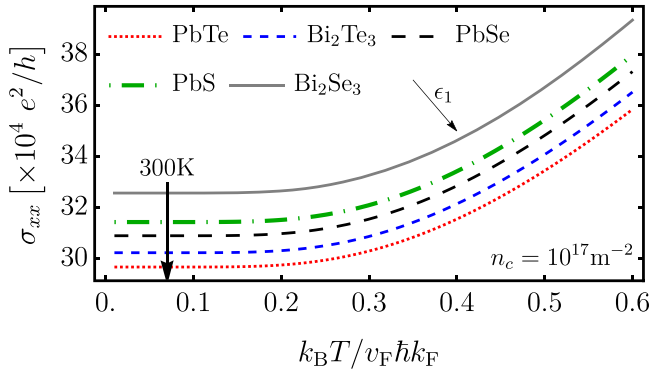


FIG. 9. Electrical conductivity of graphene $\sigma_{xx}$ as a function of the dimensionless temperature $k_BT/v_F\hbar k_F$ for $n_c = 10^{17}$ m$^{-2}$. Each curve corresponds to different materials for the slab. The relative permittivity $\epsilon_1$ of each TI is shown in Table II. The thick and thin arrows indicate the absolute temperature $T = 300$ K and the direction in which $\epsilon_1$ increases, respectively. The impurity concentration is taken as $n_{\mathrm{imp}} = 10^{17}$ m$^{-2}$.

Figure 8 shows the DC electrical conductivity $\sigma_{xx}(T)$ computed from Eq. (57), as a function of temperature for graphene when it is close to different TI materials. Here, due to the results of Sec. VI A, we ignore the MEP $\theta$. In order to reproduce the curves for actual materials, we follow the data of Table II where the relative permittivities of the TIs are presented. As can be noticed, at higher TI permittivities the electrical conductivity decreases, consistent with the presence of a strong image charge that considerably reduces the free carrier mobility in graphene.

As may be expected, the carrier density in graphene also modifies its electrical conductivity. For instance, Fig. 9 shows $\sigma_{xx}$ for a carrier concentration of $n_c = 10^{17}$ m$^{-2}$ when the slab is built from different TIs. Again, the screening effects on the image charge are presented in the scattering process so that the conductivity decreases for higher $\epsilon_r$. Nevertheless, the electrical conductivity remains constant up to room temperature, a feature that may be used for several applications.

A similar situation is found when the slab material is changed to a normal semiconductor (Si, GaAs, and InSb), as is shown in Fig. 10. Such behavior supports the idea of the screening effect due to the image charge on the scattered fermions. In fact, note that for the selected semiconductors, the graphene's conductivity is high compared with the case when the slab is made of a TI. This is because the former materials possess small relative permittivities (see Table III) in contrast with the latter ones that have $\epsilon_r$ of one order of magnitude higher.

TABLE II. Relative dielectric permittivity $\epsilon_r$ for several topological insulators.

| Material | $\epsilon_r$ | Ref. |
|---|---|---|
| PbTe | 414 | [29,30] |
| $Bi_2Te_3$ | 290 | [31,32] |
| PbSe | 210 | [33,34] |
| PbS | 169 | [35,36] |
| $Bi_2Se_3$ | 113 | [32,37] |

Finally, Fig. 11 displays the electrical resistivity $\rho_{xx} \equiv \sigma_{xx}^{-1}$ for graphene when the slab is made up of $Bi_2Te_3$, as a function of the impurity concentration $n_{\mathrm{imp}}$. Clearly, the conductivity increases when there are fewer ions inserted in graphene, given that the fermions have a larger free mean path, as can be directly appreciated from Eq. (56) where the transport relaxation time is clearly inversely proportional to the impurity concentration $n_{\mathrm{imp}}$.

## VII. SUMMARY AND CONCLUSIONS

In this work, we studied the electromagnetic coupling in a heterostructure made of a TI slab in contact with a graphene monolayer, the later with a diluted concentration of ionized impurities. By taking into account the topologically nontrivial response due to the presence of the MEP terms in the TI, we studied the configuration of the local electromagnetic fields, including the effects of the image charges and the electronic screening due to the presence of the ionized impurities in

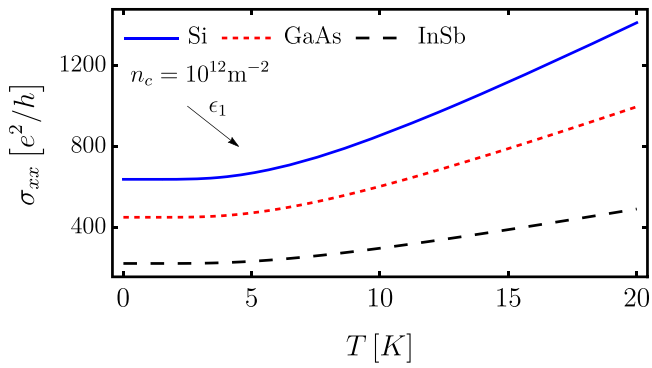


FIG. 10. Electrical conductivity of graphene as a function of temperature. Each curve corresponds to different semiconductor materials for the slab. The relative permittivity of the materials is shown in Table II. The arrow points the direction in which $\epsilon_1$ increases. The impurity concentration is taken as $n_{\mathrm{imp}} = 10^{12}$ m$^{-2}$.

TABLE III. Relative dielectric permittivity $\epsilon_r$ for several semiconductors.

| Material | $\epsilon_r$ | Ref. |
|---|---|---|
| Si | 11.9 | [38,39] |
| GaAs | 13.18 | [40,41] |
| InSb | 17.6 | [42,43] |

graphene. As a probe for this electromagnetic coupling, we used Kubo's linear response formalism to calculate the electrical conductivity at finite temperature in graphene under this configuration. To test this theory in a realistic scenario, we evaluated our analytical formulas for the characteristic parameters of several TI materials. Our result suggest that the contribution to the conductivity arising from the topologically nontrivial MEP terms are in general quite small, except at very low temperatures and large carrier densities in the graphene monolayer. On the other hand, it was also shown that the difference between the dielectric constants, expressed by the combination $(\epsilon_2-\epsilon_1)/(\epsilon_2+\epsilon_1)$ possesses an important role at determining the overall magnitude of the electrical conductivity, as can be inferred from our analytical theory since it represents the magnitude of an effective image charge located at the TI slab. We tested this effect by considering the realistic parameters for several different TI materials (Table II), including also for comparison the coupling with a few common semiconductors Si, GaAs, and InSb (see Fig. 10). In all those cases, the dominant effect of the relative dielectric permittivity of the slab material on the electrical conductivity of the coupled graphene monolayer is verified. This rather robust effect suggest a mechanism to control and modulate the electronic transport properties in this type of heterostructures. A remaining open question is whether it is possible to enhance the topological effects on the electric transport in graphene. As suggested by previous work developed by some of us [44–47], the presence of torsional strain in graphene (and possibly Weyl semimetals) in combination with an external magnetic field (such as the one generated by the MEP) leads to a chiral symmetry breaking of the massless charge carriers, with a corresponding chiral/helicity polarization of the current. This may indeed lead to an enhancement

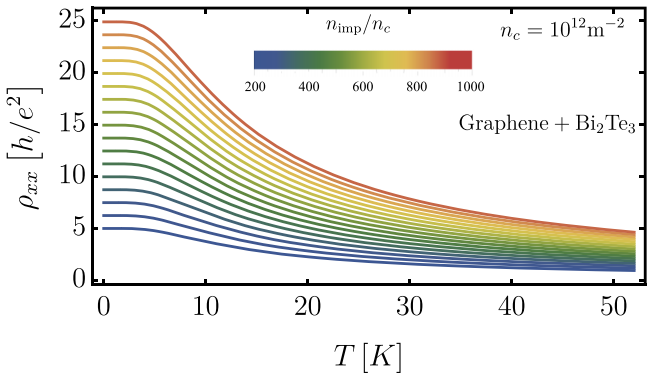


FIG. 11. Electrical resistivity of graphene as a function of temperature and the ionized impurity concentration $n_{\rm imp}$. Here is assumed that graphene is close to a $Bi_2Te_3$ slab.

of the role of the topological terms in the electronic transport coefficients, as a probe for such effects [45], and it constitutes work under current development to be communicated in a following article.

## ACKNOWLEDGMENTS

J.D.C.-Y. and E.M. acknowledge financial support from ANID PIA Anillo ACT/192023. E.M. also acknowledges financial support from Fondecyt 1230440. D.A.B. was funded by the ANID Beca Doctorado Nacional 2018 Grant No. 21180547. A.M.-R. has been partially supported by DGAPA-UNAM Project No. IA102722 and by Project CONACyT (México) No. 428214.

## APPENDIX A: CALCULATION OF THE ELECTROMAGNETIC POTENTIALS

In Sec. II we presented a detailed derivation of the electromagnetic response of the TI material, as expressed by Eq. (16) for the scalar potential and Eq. (18) for the vector potential, respectively.

The scalar potential is given by Eq. (4) with the charge density of Eq. (11), i.e., $\Phi(\mathbf{r})=\int \mathcal{G}(\mathbf{r},\mathbf{r}')\,\rho_Y(\mathbf{r}')\,d^3\mathbf{r}'$. After performing the integration over the Dirac's deltas associated with the localized ionized impurity and the screening cloud at the graphene monolayer (located at $z=z_0$), we obtain

$$\Phi(\boldsymbol{R}) = \frac{Q}{4\pi\epsilon_2}\left[\frac{1}{R}+\frac{\kappa}{\sqrt{R^2+(2z_0)^2}}\right] - \frac{1}{4\pi\epsilon_1}\frac{Q}{2\pi l_0}\int\left[\frac{1}{\sqrt{(x-x')^2+(y-y')^2}} + \frac{\kappa}{\sqrt{(x-x')^2+(y-y')^2+(2z_0)^2}}\right]\frac{e^{-R'/l_0}}{R'}d^2\mathbf{r}', \tag{A1}$$

where $R'=\sqrt{x'^2+y'^2}$. This expression suggests the definition of the generic integrals (for $j=0,\ 1$)

$$\mathcal{I}_j(R) = \frac{1}{2\pi l_0}\int d^2\mathbf{r}'\frac{e^{-R'/l_0}}{R'\sqrt{(x-x')^2+(y-y')^2+(2jz_0)^2}}, \tag{A2}$$

such that the scalar potential contains both $\mathcal{I}_0$ and $\mathcal{I}_1$. To evaluate these integrals, we use the expansion:

$$\frac{1}{\sqrt{(x-x')^2+(y-y')^2+(2jz_0)^2}} = \sum_{m=-\infty}^{+\infty}\int_0^\infty dk\, e^{im(\varphi-\varphi')}J_m(kR)J_m(kR')e^{-k(2jz_0)}, \tag{A3}$$

so that

$$\mathcal{I}_j(R) = \frac{1}{2\pi l_0}\sum_{m=-\infty}^{+\infty}\int_0^\infty dk\, J_m(kR)\,e^{-k(2jz_0)} \times\int_0^{2\pi}d\varphi'\,e^{im(\varphi-\varphi')}\int_0^\infty dR'\,J_m(kR')\,e^{-R'/l_0}. \tag{A4}$$

The angular integration yields $2\pi\delta_{m0}$. Therefore

$$\mathcal{I}_j(R) = \frac{1}{l_0}\int_0^\infty dk\, J_0(kR)e^{-k(2jz_0)}\int_0^\infty dR'\, J_0(kR')e^{-R'/l_0}. \tag{A5}$$

Now, using the integral formula

$$\int_0^\infty dx\, e^{-\alpha x}J_\nu(\beta x) = \frac{\beta^{-\nu}[\sqrt{\alpha^2+\beta^2}-\alpha]^\nu}{\sqrt{\alpha^2+\beta^2}}, \tag{A6}$$

for $\mathrm{Re}(\alpha \pm i\beta) > 0$ and $\mathrm{Re}\,\nu > -1$, we obtain

$$\mathcal{I}_j(R) = \int_0^\infty dk\, \frac{J_0(kR)}{\sqrt{1+(kl_0)^2}}\, e^{-k(2jz_0)}. \tag{A7}$$

The case $j = 0$ has a closed form expression:

$$\mathcal{I}_0(R) = \int_0^\infty dk\, \frac{J_0(kR)}{\sqrt{1+(kl_0)^2}} = \frac{1}{l_0}\, I_0(R/2l_0)\, K_0(R/2l_0), \tag{A8}$$

where $I_n(z)$ and $K_n(z)$ are the modified Bessel functions of the first and second kind, respectively. The case $j = 1$ cannot be expressed in terms of simple functions, but it can easily be evaluated numerically. All in all, the above results fully provide the scalar potential of Eq. (16). For later use we further define the functions (for $j = 0,\ 1$, respectively)

$$\Lambda_j^{(\nu)}(R) = \int_0^\infty dk\, \frac{J_\nu(kR)}{\sqrt{1+(kl_0)^2}}\, e^{-k(2jz_0)}, \tag{A9}$$

such that $\Lambda_j^{(0)}(R) = \mathcal{I}_j(R)$.

We now turn to the evaluation of the vector potential, which is given by Eq. (7) with the charge density of Eq. (11), i.e., $\mathbf{A}(\mathbf{r}) = \int \mathbf{G}(\mathbf{r},\mathbf{r}')\,\rho_Y(\mathbf{r}')\,d^3\mathbf{r}'$. To this end, we use the following integral identity [17]:

$$\begin{aligned}\frac{\mathbf{R}}{R^2}\left[1-\frac{z+z'}{\sqrt{R^2+(z+z')^2}}\right] &= \frac{1}{2\pi i}\int \frac{\mathbf{k}}{k^2}e^{-k(z+z')}e^{i\mathbf{k}\cdot\mathbf{R}}d^2\mathbf{k}\\ &= -\frac{1}{2\pi}\nabla_\perp\int\frac{1}{k^2}e^{-k(z+z')}e^{i\mathbf{k}\cdot\mathbf{R}}\,d^2\mathbf{k},\end{aligned} \tag{A10}$$

where $\nabla_\perp = \hat{\mathbf{e}}_x\partial_x + \hat{\mathbf{e}}_y\partial_y$ is the gradient in the transverse coordinates and $\mathbf{R} \equiv \boldsymbol{R} - \boldsymbol{R}' = (x-x')\hat{\mathbf{e}}_x + (y-y')\hat{\mathbf{e}}_y$. Using this result, the vector Green's function (8) can be expressed as

$$\mathbf{G}(\mathbf{r},\mathbf{r}') = -\frac{\mu_2 g}{8\pi^2}\,\hat{\mathbf{e}}_z\times\nabla_\perp\int\frac{1}{k^2}e^{-k(z+z')}e^{i\mathbf{k}\cdot\mathbf{R}}\,d^2\mathbf{k}, \tag{A11}$$

such that the vector potential becomes

$$\mathbf{A}(\mathbf{r}) = -\frac{\mu_2 g}{8\pi^2}\,\hat{\mathbf{e}}_z\times\nabla_\perp\int\frac{d^2\mathbf{k}}{k^2}\,e^{i\mathbf{k}\cdot\boldsymbol{R}}\,e^{-kz}\int d^3\mathbf{r}'\,\rho_Y(\mathbf{r}')\,e^{-i\mathbf{k}\cdot\boldsymbol{R}'}\,e^{-kz'}. \tag{A12}$$

Substituting the charge density distribution Eq. (11), and performing the integrals involving the Dirac deltas we obtain

$$\mathbf{A}(\mathbf{r}) = -\frac{\mu_2 Qg}{8\pi^2}\,\hat{\mathbf{e}}_z\times\nabla_\perp\int\frac{d^2\mathbf{k}}{k^2}\,e^{i\mathbf{k}\cdot\boldsymbol{R}}\,e^{-k(z+z_0)}\left[1-\frac{1}{l_0}\int_0^\infty dR'\,J_0(kR')\,e^{-R'/l_0}\right]. \tag{A13}$$

The integral in $R'$ can be easily evaluated by using the formula (A6). To evaluate this integral we introduce polar coordinates such that $\mathbf{k}\cdot\boldsymbol{R} = kR\cos\varphi$. Performing the angular integration we obtain

$$\mathbf{A}(\mathbf{r}) = -\frac{\mu_2 Qg}{4\pi}\,\hat{\mathbf{e}}_z\times\nabla_\perp\int\frac{dk}{k}\,J_0(kR)\,e^{-k(z+z_0)}\left[1-\frac{1}{\sqrt{1+(kl_0)^2}}\right]. \tag{A14}$$

Finally, taking the gradient, $-\nabla_\perp J_0(kR) = k\,\hat{\mathbf{e}}_R J_1(kR)$, and using that $\hat{\mathbf{e}}_z\times\hat{\mathbf{e}}_R = \hat{\mathbf{e}}_\phi$, one finds that at the plane $z = z_0$, where $\mathbf{r} = \mathbf{R} + \hat{e}_z\,z_0$,

$$\mathbf{A}(\mathbf{R}) = \frac{\mu_2 Qg}{4\pi}\,\hat{\mathbf{e}}_\phi\int_0^\infty dk\,J_1(kR)\,e^{-2kz_0}\left[1-\frac{1}{\sqrt{1+(kl_0)^2}}\right]. \tag{A15}$$

The first integral can be evaluated by using the integral formula (A6) and yields the Schwinger vector potential for a magnetic monopole at the image point $-z_0$. It corresponds to the first term in Eq. (18). The second term cannot be expressed in terms of simple functions; however, it corresponds to the function $\Lambda_1^{(1)}(R)$, defined by Eq. (A9). On the whole we get the expression (18) for the vector potential.

## APPENDIX B: THE SCATTERED STATES

### 1. The Lippman-Schwinger equation and free Green's function

In this section, we shall closely follow the formalism presented in Ref. [12]. In the elastic scattering theory, we look for spinor solutions $|\Psi_{\mathbf{k},\lambda}\rangle$ of the total Hamiltonian of Eq. (25) with the same energy as in Eq. (27). That solution is given by the well known Lippmann-Schwinger equation

$$|\Psi_{\mathbf{k},\lambda}\rangle = |\Phi_{\mathbf{k},\lambda}\rangle + \hat{G}_{R,0}^{(\lambda,\xi)}(E)\hat{H}_1^\xi|\Psi_{\mathbf{k},\lambda}\rangle, \tag{B1}$$

where the Green's operator $\hat{G}_{R,0}^{(\lambda,\xi)}(E)$ or *resolvent* is given by

$$\hat{G}_{R,0}^{(\lambda,\xi)}(E) = \frac{1}{E-\hat{H}_0^\xi+i\eta^+}, \tag{B2}$$

where the positive sign for the regulator $i\eta^+$ defines the retarded Green's function (GF), which in turn produces outgoing spherical waves from the scattering center. Moreover, the advanced GF is defined as

$$\hat{G}_{A,0}^{(\lambda,\xi)}(E) = \left[\hat{G}_{R,0}^{(\lambda,\xi)}(E)\right]^\dagger, \tag{B3}$$

and using the explicit form of the resolvent of Eq. (B2) we have a relation between the retarded and the advanced GFs

$$\hat{G}^{(\lambda,\xi)}_{R,0}(E) - \hat{G}^{(\lambda,\xi)}_{A,0}(E) = -2\pi i\delta\big(E - \hat{H}^{\xi}_{0}\big). \tag{B4}$$

The resolvent in Eq. (B2) is the solution to the equation

$$\big(E + i\eta^{+} - \hat{H}^{\xi}_{0}\big)\hat{G}^{(\lambda,\xi)}_{R,0}(E) = \hat{I}. \tag{B5}$$

At this point we introduce the $\hat{T}$ matrix as usual

$$\hat{T}^{(\lambda,\xi)}(E)|\Phi_{\mathbf{k},\lambda}\rangle = \hat{H}^{\xi}_{1}|\Psi_{\mathbf{k},\lambda}\rangle, \tag{B6}$$

so that the Lippmann-Schwinger equation becomes

$$|\Psi_{\mathbf{k},\lambda}\rangle = \big[\hat{I} + \hat{G}^{(\lambda,\xi)}_{R,0}(E)\hat{T}^{(\lambda,\xi)}(E)\big]|\Phi_{\mathbf{k},\lambda}\rangle. \tag{B7}$$

Inserting Eq. (B7) into Eq. (B6), and solving for the $\hat{T}$-matrix operator, we find the formal expression

$$\hat{T}^{(\lambda,\xi)}(E) = \hat{H}^{\xi}_{1}\big[\hat{I} - \hat{G}^{(\lambda,\xi)}_{R,0}(E)\hat{H}^{\xi}_{1}\big]^{-1}. \tag{B8}$$

We are also interested in the total retarded GF, which is the solution to the equation

$$(E + i\eta^{+} - \hat{H}^{\xi})\hat{G}^{(\lambda,\xi)}_{R}(E) = \hat{I}, \tag{B9}$$

where $\hat{H}^{\xi} = \hat{H}^{\xi}_{0} + \hat{H}^{\xi}_{1}$ is the full Hamiltonian. The last equation can be transformed into a self-consistent relation

$$\big(E + i\eta^{+} - \hat{H}^{\xi}_{0}\big)\hat{G}^{(\lambda,\xi)}_{R}(E) = \hat{I} + \hat{H}^{\xi}_{1}\hat{G}^{(\lambda,\xi)}_{R}(E), \tag{B10}$$

and making use of Eq. (B5) we have

$$\hat{G}^{(\lambda,\xi)}_{R}(E) = \hat{G}^{(\lambda,\xi)}_{R,0}(E) + \hat{G}^{(\lambda,\xi)}_{R,0}(E)\hat{H}^{\xi}_{1}\hat{G}^{(\lambda,\xi)}_{R}(E). \tag{B11}$$

The formal solution of this equation is

$$\hat{G}^{(\lambda,\xi)}_{R}(E) = \big[\hat{I} - \hat{G}^{(\lambda,\xi)}_{R,0}(E)\hat{H}^{\xi}_{1}\big]^{-1}\hat{G}^{(\lambda,\xi)}_{R,0}(E), \tag{B12}$$

that combined with Eq. (B8) leads to the identity

$$\hat{H}^{\xi}_{1}\hat{G}^{(\lambda,\xi)}_{R}(E) = \hat{T}^{(\lambda,\xi)}(E)\hat{G}^{(\lambda,\xi)}_{R,0}(E). \tag{B13}$$

Then, the complete retarded GF is given by

$$\hat{G}^{(\lambda,\xi)}_{R}(E) = \hat{G}^{(\lambda,\xi)}_{R,0}(E) + \hat{G}^{(\lambda,\xi)}_{R,0}(E)\hat{T}^{(\lambda,\xi)}(E)\hat{G}^{(\lambda,\xi)}_{R,0}(E), \tag{B14}$$

and hence one can show that the $T$ matrix itself satisfies a self-consistent equation of the form

$$\hat{T}^{(\lambda,\xi)}(E) = \hat{H}^{\xi}_{1} + \hat{H}^{\xi}_{1}\hat{G}^{(\lambda,\xi)}_{R,0}(E)\hat{T}^{(\lambda,\xi)}(E). \tag{B15}$$

From the latter, it follows that

$$\hat{T}^{(\lambda,\xi)}(E) - [\hat{T}^{(\lambda,\xi)}(E)]^{\dagger} = [\hat{T}^{(\lambda,\xi)}(E)]^{\dagger}\big[\hat{G}^{(\lambda,\xi)}_{R}(E) - \hat{G}^{\xi}_{A}(E)\big]\hat{T}^{(\lambda,\xi)}(E), \tag{B16}$$

and using the Eq. (B4) we get an useful expression:

$$\hat{T}^{(\lambda,\xi)}(E) - [\hat{T}^{(\lambda,\xi)}(E)]^{\dagger} = -2\pi i[\hat{T}^{(\lambda,\xi)}(E)]^{\dagger}\delta\big(E - \hat{H}^{\xi}_{0}\big)\hat{T}^{(\lambda,\xi)}(E). \tag{B17}$$

The form for the retarded Green's function matrix in the coordinates representation is [12]

$$\mathbf{G}^{(\lambda,\xi)}_{R,0}(\mathbf{R},\mathbf{R}';k) = -\frac{\lambda\xi ik}{4\hbar v_F}\begin{bmatrix} H^{(1)}_{0}(k|\mathbf{R}-\mathbf{R}'|) & i\lambda e^{-i\varphi}H^{(1)}_{1}(k|\mathbf{R}-\mathbf{R}'|) \\ i\lambda e^{i\varphi}H^{(1)}_{1}(k|\mathbf{R}-\mathbf{R}'|) & H^{(1)}_{0}(k|\mathbf{R}-\mathbf{R}'|)\end{bmatrix}, \tag{B18}$$

where $\varphi$ is the angle of the vector $\mathbf{R}-\mathbf{R}'$ with respect to the $x$ axis. We want to expand this matrix Green's function in polar coordinates. In order to do it, we use the addition theorem for Bessel functions [48],

$$e^{\pm iv\psi}Z_{v}(k|\mathbf{R}-\mathbf{R}'|) = \sum_{m=-\infty}^{\infty} Z_{v+m}(kR)J_{m}(kR')e^{\pm im\theta}, \tag{B19}$$

where $Z_v$ is any of the Bessel functions $J_v$, $Y_v$, $H^{(1)}_v$, or $H^{(2)}_v$. Here $R$, $R'$, represent $|\mathbf{R}|$, $|\mathbf{R}'|$, respectively. Moreover, the angles $\theta$ and $\psi$ are defined in the triangle of Fig. 12, from which

$$\varphi = 2\pi + \phi - \psi. \tag{B20}$$

Let us write the Green's function as:

$$\mathbf{G}^{(\lambda,\xi)}_{R,0}(\mathbf{R},\mathbf{R}';k) = -\frac{\lambda\xi ik}{4\hbar v_F}\begin{bmatrix} G_{11} & G_{12} \\ G_{21} & G_{22}\end{bmatrix}. \tag{B21}$$

We first consider the case $R > R'$. So that, by using Eq. (B19) we have for the component $G_{11}$

$$\begin{aligned} G_{11} &= H^{(1)}_{0}(k|\mathbf{R}-\mathbf{R}'|) \\ &= \sum_{m=-\infty}^{\infty} H^{(1)}_{m}(kR)J_{m}(kR')e^{im(\phi'-\phi)} \\ &= \sum_{m=-\infty}^{\infty} H^{(1)}_{-m}(kR)J_{-m}(kR')e^{-im(\phi'-\phi)} \\ &= \sum_{m=-\infty}^{\infty} H^{(1)}_{m}(kR)J_{m}(kR')e^{im(\phi-\phi')}, \end{aligned} \tag{B22}$$

where in the third line we made the replacement $m \to -m$ and use the property $Z_{-n}(u) = (-1)^n Z_n(u)$, valid for Bessel functions when $n \in \mathbb{Z}$. For latter convenience, the component $G_{22}$ is obtained by shifting $m$ in Eq. (B22) as $m \to m+1$.

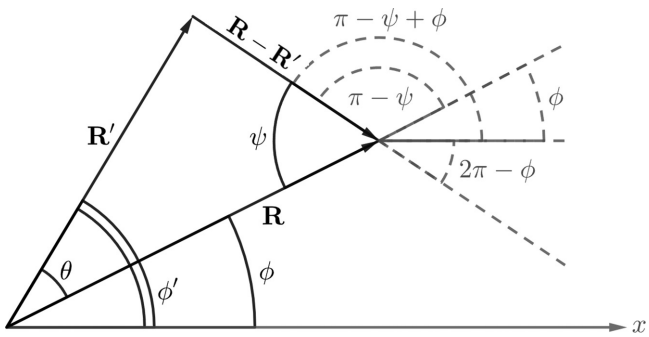


FIG. 12. Triangle used for the application of the addition theorem for the Bessel functions.

We get

$$G_{22} = \sum_{m=-\infty}^{\infty} H_{m+1}^{(1)}(kR) J_{m+1}(kR') e^{i(m+1)(\phi-\phi')}. \quad \text{(B23)}$$

On the other hand:

$$\begin{aligned} G_{21} &= i\lambda e^{i\varphi} H_1^{(1)}(k|\mathbf{R}-\mathbf{R}'|) \\ &= i\lambda e^{i(2\pi+\phi-\psi)} H_1^{(1)}(k|\mathbf{R}-\mathbf{R}'|) \\ &= i\lambda e^{i\phi} e^{-i\psi} H_1^{(1)}(k|\mathbf{R}-\mathbf{R}'|) \\ &= i\lambda e^{i\phi} \sum_{m=-\infty}^{\infty} H_{m+1}^{(1)}(kR) J_m(kR') e^{-im(\phi'-\phi)} \\ &= i\lambda \sum_{m=-\infty}^{\infty} H_{m+1}^{(1)}(kR) J_m(kR') e^{i\phi} e^{im(\phi-\phi')}, \end{aligned} \quad \text{(B24)}$$

and

$$\begin{aligned} G_{12} &= i\lambda e^{-i\varphi} H_1^{(1)}(k|\mathbf{R}-\mathbf{R}'|) \\ &= i\lambda e^{-i(2\pi+\phi-\psi)} H_1^{(1)}(k|\mathbf{R}-\mathbf{R}'|) \\ &= i\lambda e^{-i\phi} \sum_{m=-\infty}^{\infty} H_{m+1}^{(1)}(kR) J_m(kR') e^{im(\phi'-\phi)} \\ &= i\lambda \sum_{m=-\infty}^{\infty} H_{-m}^{(1)}(kR) J_{-m-1}(kR') e^{-i\phi} e^{-i(-m-1)(\phi-\phi')} \\ &= -i\lambda \sum_{m=-\infty}^{\infty} H_m^{(1)}(kR) J_{m+1}(kR') e^{-i\phi'} e^{im(\phi-\phi')}, \end{aligned} \quad \text{(B25)}$$

where in the last step we shifted $m \to -m-1$. Thus, we have obtained the four components for the Green's function matrix for the case $R > R'$. A similar procedure for the case $R < R'$ allows us to write the Green's function as

$$\mathbf{G}_{R,0}^{(\lambda,\xi)}(\mathbf{R},\mathbf{R}';k) = -\frac{\lambda\xi ik}{4\hbar v_F} \sum_{m\in\mathbb{Z}} \begin{bmatrix} J_m(kR_<)H_m^{(1)}(kR_>)e^{im(\phi-\phi')} & -i\lambda J_{m+1}(kR_<)H_m^{(1)}(kR_>)e^{-i\phi'}e^{im(\phi-\phi')} \\ i\lambda J_m(kR_<)H_{m+1}^{(1)}(kR_>)e^{i\phi}e^{im(\phi-\phi')} & J_{m+1}(kR_<)H_{m+1}^{(1)}(kR_>)e^{i(m+1)(\phi-\phi')} \end{bmatrix}, \quad \text{(B26)}$$

where $R_>$ ($R_<$) is the greater (lower) between $R$ and $R'$.

### 2. The radial integral equation

Now, representing the Lippmann-Schwinger Eq. (B1) in the coordinate basis we have

$$\begin{aligned} \langle \mathbf{R}|\Psi_{\mathbf{k},\lambda}\rangle &= \langle \mathbf{R}|\Phi_{\mathbf{k},\lambda}\rangle \\ &+ \int_{\mathbb{R}^2} d^2R'\, \mathbf{G}_{R,0}^{(\lambda,\xi)}(\mathbf{R},\mathbf{R}';k)\mathbf{H}_1^{\xi}(\mathbf{R}')\langle \mathbf{R}'||\Psi_{\mathbf{k},\lambda}\rangle, \end{aligned} \quad \text{(B27)}$$

where $\langle \mathbf{R}|\Psi_{\mathbf{k},\lambda}\rangle$ is given in Eq. (30), $\langle \mathbf{R}|\Phi_{\mathbf{k},\lambda}\rangle$ is the free spinor of Eq. (29), $\mathbf{G}_{R,0}^{(\lambda,\xi)}(\mathbf{R},\mathbf{R}';k)$ is the matrix Green's function given in Eq. (B26), and the matrix form of the operator representing the interaction with the external fields $\mathbf{H}_1^{\xi}$ is

$$\mathbf{H}_1^{\xi}(\mathbf{R}) = -\xi q v_F \boldsymbol{\sigma}\cdot\hat{\boldsymbol{e}}_\phi A(\mathbf{R}) + q\Phi(\mathbf{R})\sigma_0, \quad \text{(B28)}$$

where the scalar potential $\Phi(\mathbf{R})$ is given in Eq. (16), the magnitude of the vector potential $\mathbf{A}(\mathbf{R}) = \hat{\boldsymbol{e}}_\phi A(\mathbf{R})$ is given in Eq. (18), $\sigma_0$ is the $2\times 2$ unit matrix and

$$\boldsymbol{\sigma}\cdot\hat{\boldsymbol{e}}_\phi = \begin{bmatrix} 0 & -ie^{-i\phi} \\ ie^{i\phi} & 0 \end{bmatrix}. \quad \text{(B29)}$$

Then, we have

$$\mathbf{H}_1^{\xi}(\mathbf{R}) = \begin{bmatrix} q\Phi(R) & ie^{-i\phi}\xi q v_F A(R) \\ -ie^{i\phi}\xi q v_F A(R) & q\Phi(R) \end{bmatrix}. \quad \text{(B30)}$$

After we make all the replacements, we can extract the radial part to obtain the radial integral equation. For $R < a$ the final result can be written as

$$\begin{aligned} \begin{bmatrix} f_m(R) \\ g_m(R) \end{bmatrix} &= \begin{bmatrix} J_m(kR) \\ J_{m+1}(kR) \end{bmatrix} - \frac{\lambda\xi i\pi k}{2\hbar v_F} \int_0^R dR'R' \begin{bmatrix} J_m(kR')H_m^{(1)}(kR) & J_{m+1}(kR')H_m^{(1)}(kR) \\ J_m(kR')H_{m+1}^{(1)}(kR) & J_{m+1}(kR')H_{m+1}^{(1)}(kR) \end{bmatrix} \begin{bmatrix} e\Phi(R') & -\lambda\xi q v_F A(R') \\ -\lambda\xi q v_F A(R') & e\Phi(R') \end{bmatrix} \begin{bmatrix} f_m(R') \\ g_m(R') \end{bmatrix} \\ &- \frac{\lambda\xi i\pi k}{2\hbar v_F} \int_R^a dR'R' \begin{bmatrix} J_m(kR)H_m^{(1)}(kR') & J_{m+1}(kR)H_m^{(1)}(kR') \\ J_m(kR)H_{m+1}^{(1)}(kR') & J_{m+1}(kR)H_{m+1}^{(1)}(kR') \end{bmatrix} \begin{bmatrix} e\Phi(R') & -\lambda\xi q v_F A(R') \\ -\lambda\xi q v_F A(R') & e\Phi(R') \end{bmatrix} \begin{bmatrix} f_m(R') \\ g_m(R') \end{bmatrix}. \end{aligned} \quad \text{(B31)}$$

and for $R > a$ we have

$$\begin{bmatrix} f_m(R) \\ g_m(R) \end{bmatrix} = \begin{bmatrix} J_m(kR) \\ J_{m+1}(kR) \end{bmatrix} - \frac{\lambda\xi i\pi k}{2\hbar v_F} \int_0^a dR'R' \begin{bmatrix} J_m(kR')H_m^{(1)}(kR) & J_{m+1}(kR')H_m^{(1)}(kR) \\ J_m(kR')H_{m+1}^{(1)}(kR) & J_{m+1}(kR')H_{m+1}^{(1)}(kR) \end{bmatrix} \begin{bmatrix} e\Phi(R') & -\lambda\xi e v_F A(R') \\ -\lambda\xi e v_F A(R') & e\Phi(R') \end{bmatrix} \begin{bmatrix} f_m(R') \\ g_m(R') \end{bmatrix}. \quad \text{(B32)}$$

Finally, in order to obtain asymptotic eigenstates, we expand the Bessel's functions when $x \to \infty$ as follows:

$$J_\nu(x) \to \sqrt{\frac{1}{2\pi x}}[e^{i(x-\frac{\nu\pi}{2}-\frac{\pi}{4})} + e^{-i(x-\frac{\nu\pi}{2}-\frac{\pi}{4})}],$$
$$H_\nu^{(1)}(x) \to \sqrt{\frac{2}{\pi x}} e^{i\left(x-\frac{\nu\pi}{2}-\frac{\pi}{4}\right)}. \tag{B33}$$

Then

$$\begin{bmatrix} J_m(kR) \\ J_{m+1}(kR) \end{bmatrix} \to \sqrt{\frac{2}{\pi kR}} \sum_{s=\pm 1} \begin{bmatrix} 1 \\ \mp is \end{bmatrix} e^{\pm is(kR-\frac{m\pi}{2}-\frac{\pi}{4})}, \tag{B34}$$

and

$$\begin{bmatrix} J_m(kR')H_m^{(1)}(kR) & J_{m+1}(kR')H_m^{(1)}(kR) \\ J_m(kR')H_{m+1}^{(1)}(kR) & J_{m+1}(kR')H_{m+1}^{(1)}(kR) \end{bmatrix}$$
$$\to \sqrt{\frac{2}{\pi k}} \begin{bmatrix} 1 \\ -i \end{bmatrix} [J_m(kR') \quad J_{m+1}(kR')] \frac{e^{i\left(kR-\frac{m\pi}{2}-\frac{\pi}{4}\right)}}{\sqrt{R}}. \tag{B35}$$

so that after replacing in Eq. (B32), we obtain the result shown in Eq. (33).

## APPENDIX C: THE TRANSPORT COEFFICIENTS

In this section, we shall present the mathematical details involved in the calculation of the electronic transport coefficients, in particular the electrical conductivity, leading to the results presented in the main body of the article.

### 1. The Onsager's coefficients

In order to compute the microscopic transport coefficients, let us start by defining the quantum operators representing the particle, energy, and heat currents, respectively:

$$\hat{\mathbf{j}} = \sum_{\mathbf{p}\sigma} \mathbf{v}_\mathbf{p} \hat{n}_{\mathbf{p}\sigma}, \tag{C1}$$
$$\hat{\mathbf{j}}_E = \sum_{\mathbf{p}\sigma} \mathbf{v}_\mathbf{p} \mathcal{E}_{\mathbf{p}\sigma} \hat{n}_{\mathbf{p}\sigma}, \tag{C2}$$
$$\hat{\mathbf{j}}_Q = \sum_{\mathbf{p}\sigma} \mathbf{v}_\mathbf{p} (\mathcal{E}_{\mathbf{p}\sigma} - \mu) \hat{n}_{\mathbf{p}\sigma}, \tag{C3}$$

where for a particle with momentum $\mathbf{p}$ and spin $\sigma$, we identify $\mathcal{E}_{\mathbf{p}\sigma}$ as the particle's energy, $\mathbf{v}_\mathbf{p} = -\nabla_\mathbf{p}\mathcal{E}_{\mathbf{p}\sigma}$ as the group velocity at momentum $\mathbf{p}$, $\hat{n}_{\mathbf{p}\sigma}$ as the particle number density operator, and $\mu$ as the chemical potential of the system. The corresponding observed macroscopic currents are given by the ensemble average of the above operators, i.e.,

$$\mathbf{J} = \langle \hat{\mathbf{j}} \rangle, \tag{C4a}$$
$$\mathbf{J}_E = \langle \hat{\mathbf{j}}_E \rangle, \tag{C4b}$$
$$\mathbf{J}_Q = \langle \hat{\mathbf{j}}_Q \rangle. \tag{C4c}$$

Now, let us introduce the Onsager's coefficients $L_{\alpha\beta}^{(ij)}$ through the relations linking the currents with the gradients in temperature and electrochemical potential [23]

$$J_\alpha = -\frac{1}{T} L_{\alpha\beta}^{(11)} \nabla_\beta (\mu + eV) + L_{\alpha\beta}^{(12)} \nabla_\beta \left(\frac{1}{T}\right), \tag{C5a}$$
$$J_{Q\alpha} = -\frac{1}{T} L_{\alpha\beta}^{(21)} \nabla_\beta (\mu + eV) + L_{\alpha\beta}^{(22)} \nabla_\beta \left(\frac{1}{T}\right), \tag{C5b}$$

which in tensor notation take the form

$$\mathbf{J} = -\frac{1}{T} \overleftrightarrow{\mathbf{L}}^{(11)} \cdot \nabla(\mu + eV) + \overleftrightarrow{\mathbf{L}}^{(12)} \cdot \nabla\left(\frac{1}{T}\right), \tag{C6a}$$
$$\mathbf{J}_Q = -\frac{1}{T} \overleftrightarrow{\mathbf{L}}^{(21)} \cdot \nabla(\mu + eV) + \overleftrightarrow{\mathbf{L}}^{(22)} \cdot \nabla\left(\frac{1}{T}\right). \tag{C6b}$$

The above tensors are directly related to the transport coefficients, as can be shown by exploring different limits [23]. First, note that for $\nabla T = 0$ and $\nabla \mu = 0$, the current is purely electric. Therefore:

$$e\mathbf{J} = -\frac{1}{T} \overleftrightarrow{\mathbf{L}}^{(11)} \cdot \nabla(e^2 V) = \overleftrightarrow{\boldsymbol{\sigma}} \cdot (-\nabla V), \tag{C7}$$

and the electrical conductivity tensor is given by

$$\overleftrightarrow{\boldsymbol{\sigma}} = \frac{e^2}{T} \overleftrightarrow{\mathbf{L}}^{(11)}. \tag{C8}$$

The same procedure is applied to find the thermal conductivity, which is given by the condition $\mathbf{J} = 0$. Thus, from Eq. (C6a) we have

$$\mathbf{0} = -\frac{1}{T} \overleftrightarrow{\mathbf{L}}^{(11)} \cdot \nabla(\mu + eV) + \overleftrightarrow{\mathbf{L}}^{(12)} \cdot \nabla\left(\frac{1}{T}\right), \tag{C9}$$

and solving we obtain

$$\frac{1}{T}\nabla(\mu + eV) = [\overleftrightarrow{\mathbf{L}}^{(11)}]^{-1} \cdot \overleftrightarrow{\mathbf{L}}^{(12)} \cdot \nabla\left(\frac{1}{T}\right). \tag{C10}$$

By substituting in Eq. (C6b) we have

$$\mathbf{J}_Q = -\overleftrightarrow{\mathbf{L}}^{(21)} \cdot [\overleftrightarrow{\mathbf{L}}^{(11)}]^{-1} \cdot \overleftrightarrow{\mathbf{L}}^{(12)} \cdot \nabla\left(\frac{1}{T}\right) + \overleftrightarrow{\mathbf{L}}^{(22)} \cdot \nabla\left(\frac{1}{T}\right)$$
$$= -\frac{1}{T^2}(\overleftrightarrow{\mathbf{L}}^{(22)} - \overleftrightarrow{\mathbf{L}}^{(21)} \cdot [\overleftrightarrow{\mathbf{L}}^{(11)}]^{-1} \cdot \overleftrightarrow{\mathbf{L}}^{(12)}) \cdot \nabla T. \tag{C11}$$

Then, the thermal conductivity tensor is

$$\overleftrightarrow{\boldsymbol{\kappa}} = \frac{1}{T^2}(\overleftrightarrow{\mathbf{L}}^{(22)} - \overleftrightarrow{\mathbf{L}}^{(21)} \cdot [\overleftrightarrow{\mathbf{L}}^{(11)}]^{-1} \cdot \overleftrightarrow{\mathbf{L}}^{(12)}), \tag{C12}$$

and the Seebeck coefficient (thermopower) is given by

$$S = \frac{1}{eT} [\overleftrightarrow{\mathbf{L}}^{(11)}]^{-1} \cdot \overleftrightarrow{\mathbf{L}}^{(12)}. \tag{C13}$$

### 2. The linear response regime

To express the Onsager's coefficients in terms of dynamical variables, we apply the Kubo formalism within the linear response regime. For that sake, we express the entropy

production rate as [23]

$$\begin{aligned}\frac{dQ}{dt} &= T\frac{\partial S}{\partial t}\\ &= -\mathbf{J}\cdot\nabla(\mu+eV)+T\,\mathbf{J}_Q\cdot\nabla\left(\frac{1}{T}\right)\\ &= T\sum_i \mathbf{J}_i\cdot\mathbf{X}_i\\ &\equiv \frac{\partial}{\partial t}F(t),\end{aligned} \tag{C14}$$

where $\mathbf{J}_1=\mathbf{J}$, $\mathbf{J}_2=\mathbf{J}_Q$, and

$$\begin{aligned}\mathbf{X}_1 &= -\frac{1}{T}\nabla(\mu+eV),\\ \mathbf{X}_2 &= \nabla\left(\frac{1}{T}\right).\end{aligned} \tag{C15}$$

We know that the Kubo's formula is given by [24]

$$\mathbf{J}_i = -\int_0^\infty dt\, e^{-st}\int_0^\beta d\beta'\,\mathrm{Tr}\left[\hat{\rho}_0\frac{\partial}{\partial t}F(-t-i\hbar\beta')\hat{\mathbf{j}}_i(\mathbf{R})\right], \tag{C16}$$

where $s$ is a positive quantity that guarantees the adiabatic switching-on of the perturbation, so that at the end of the calculation, we take the limit $s\to 0$. When inserting Eq. (C14) into Eq. (C16), we have

$$\mathbf{J}_i = -T\mathcal{L}\left\{\int_0^\beta d\beta'\,\mathrm{Tr}\left[\hat{\rho}_0\left(\sum_k \hat{\mathbf{j}}_k(-t-i\hbar\beta')\cdot\mathbf{X}_k\right)\hat{\mathbf{j}}_i(\mathbf{R})\right]\right\}, \tag{C17}$$

with $\mathcal{L}\{\cdot\}$ the Laplace's transform in the variable $s$:

$$\mathcal{L}\{f(t)\} = \int_0^\infty dt\, e^{-st}f(t). \tag{C18}$$

Then,

$$L^{(11)}_{\alpha\beta} = -T\mathcal{L}\left\{\int_0^\beta d\beta'\,\mathrm{Tr}[\hat{\rho}_0\hat{j}_\alpha(-t-i\hbar\beta')\hat{j}_\beta]\right\}, \tag{C19a}$$

$$L^{(12)}_{\alpha\beta} = L^{(21)}_{\alpha\beta} = -T\mathcal{L}\left\{\int_0^\beta d\beta'\,\mathrm{Tr}[\hat{\rho}_0\hat{j}_{Q\alpha}(-t-i\hbar\beta')\hat{j}_\beta]\right\}, \tag{C19b}$$

$$L^{(22)}_{\alpha\beta} = -T\mathcal{L}\left\{\int_0^\beta d\beta'\,\mathrm{Tr}[\hat{\rho}_0\hat{j}_{Q\alpha}(-t-i\hbar\beta')\hat{j}_{Q\beta}]\right\}. \tag{C19c}$$

To compute the traces, we define the current operator by

$$\hat{\mathbf{j}}^{(\xi)}(\mathbf{R}) = \xi v_F|\mathbf{R}\rangle\boldsymbol{\sigma}\langle\mathbf{R}|, \tag{C20}$$

the heat current operator

$$\hat{\mathbf{j}}^{(\xi)}_Q(\mathbf{R}) = \xi v_F(\hat{H}^\xi-\mu)|\mathbf{R}\rangle\boldsymbol{\sigma}\langle\mathbf{R}|, \tag{C21}$$

and the equilibrium density operator

$$\hat{\rho}_0 = \frac{\exp[-\beta(\hat{H}^\xi-\mu)]}{\mathcal{Z}(\beta,V,\mu)}, \tag{C22}$$

where $\mathcal{Z}(\beta,V,\mu)=\mathrm{Tr}\exp[-\beta(\hat{H}^\xi-\mu)]$ is the grand-canonical partition function. Here, $\hat{H}^\xi$ is the Dirac Hamiltonian with chirality $\xi$ and Fermi's velocity $v_F$.

We start with Eq. (C19a) and take the trace in the complete and orthonormal basis $\{|\Psi_{\mathbf{k},\lambda}\rangle\}$ of the total Hamiltonian, such that

$$\hat{H}^\xi|\Psi_{\mathbf{k},\lambda}\rangle = \mathcal{E}^{(\lambda,\xi)}_{\mathbf{k}}|\Psi_{\mathbf{k},\lambda}\rangle, \tag{C23}$$

from which

$$\begin{aligned}L^{(11)}_{\alpha\beta}(\mathbf{R},\mathbf{R}') &= -T\mathcal{L}\left\{\int_0^\beta d\beta'\,\mathrm{Tr}[\hat{\rho}_0\hat{j}_\alpha(\mathbf{R},-t-i\hbar\beta')\hat{j}_\beta(\mathbf{R}',0)]\right\}\\ &= -T\mathcal{L}\left\{\int_0^\beta d\beta'\,\mathrm{Tr}[\hat{\rho}_0 e^{i(-t-i\hbar\beta')\hat{H}^\xi/\hbar}\hat{j}_\alpha(\mathbf{R})e^{i(t+i\hbar\beta')\hat{H}^\xi/\hbar}\hat{j}_\beta(\mathbf{R}')]\right\}\\ &= -T\mathcal{L}\left\{\int_0^\beta d\beta'\sum_{\lambda,\lambda'}\int\frac{d^2k}{(2\pi)^2}\int\frac{d^2k'}{(2\pi)^2}\right.\\ &\quad\left.\times\,\langle\Psi_{\mathbf{k},\lambda}||\hat{\rho}_0 e^{i(-t-i\hbar\beta')\hat{H}^\xi/\hbar}\hat{j}_\alpha(\mathbf{R})e^{i(t+i\hbar\beta')\hat{H}^\xi/\hbar}||\Psi_{\mathbf{k}',\lambda'}|\rangle|\langle\Psi_{\mathbf{k}',\lambda'}||\hat{j}_\beta(\mathbf{R}')||\Psi_{\mathbf{k},\lambda}\rangle\right\}\\ &= -T\sum_{\lambda,\lambda'}\int\frac{d^2k}{(2\pi)^2}\int\frac{d^2k'}{(2\pi)^2}\int_0^\infty dt\, e^{-[i(\mathcal{E}^{(\lambda,\xi)}_{\mathbf{k}}-\mathcal{E}^{(\lambda',\xi)}_{\mathbf{k}'})/\hbar+s]t}\int_0^\beta d\beta' e^{(\mathcal{E}^{(\lambda,\xi)}_{\mathbf{k}}-\mathcal{E}^{(\lambda',\xi)}_{\mathbf{k}'})\beta'}\\ &\quad\times\,\rho_0\left(\mathcal{E}^{(\lambda,\xi)}_{\mathbf{k}}\right)\langle\Psi_{\mathbf{k},\lambda}||\hat{j}_\alpha(\mathbf{R})||\Psi_{\mathbf{k}',\lambda'}|\rangle|\langle\Psi_{\mathbf{k}',\lambda'}||\hat{j}_\beta(\mathbf{R}')||\Psi_{\mathbf{k},\lambda}\rangle\\ &= -T\sum_{\lambda,\lambda'}\int\frac{d^2k}{(2\pi)^2}\int\frac{d^2k'}{(2\pi)^2}\,\frac{-1}{-\left[i\left(\mathcal{E}^{(\lambda,\xi)}_{\mathbf{k}}-\mathcal{E}^{(\lambda',\xi)}_{\mathbf{k}'}\right)/\hbar+s\right]}\frac{e^{(\mathcal{E}^{(\lambda,\xi)}_{\mathbf{k}}-\mathcal{E}^{(\lambda',\xi)}_{\mathbf{k}'})\beta}-1}{\left(\mathcal{E}^{(\lambda,\xi)}_{\mathbf{k}}-\mathcal{E}^{(\lambda',\xi)}_{\mathbf{k}'}\right)}\\ &\quad\times\,\frac{e^{-\beta(\mathcal{E}^{(\lambda,\xi)}_{\mathbf{k}}-\mu)}}{\mathcal{Z}}\langle\Psi_{\mathbf{k},\lambda}||\hat{j}_\alpha(\mathbf{R})||\Psi_{\mathbf{k}',\lambda'}|\rangle|\langle\Psi_{\mathbf{k}',\lambda'}||\hat{j}_\beta(\mathbf{R}')||\Psi_{\mathbf{k},\lambda}\rangle.\end{aligned} \tag{C24}$$

Rearranging terms:

$$L^{(11)}_{\alpha\beta}(\mathbf{R},\mathbf{R}') = -\hbar T\sum_{\lambda,\lambda'}\int\frac{d^2k}{(2\pi)^2}\int\frac{d^2k'}{(2\pi)^2}\left[\frac{-i\left(\mathcal{E}^{(\lambda,\xi)}_{\mathbf{k}}-\mathcal{E}^{(\lambda',\xi)}_{\mathbf{k}'}\right)+\hbar s}{\left(\mathcal{E}^{(\lambda,\xi)}_{\mathbf{k}}-\mathcal{E}^{(\lambda',\xi)}_{\mathbf{k}'}\right)^2+\hbar^2s^2}\right]\left[\frac{\rho_0\left(\mathcal{E}^{(\lambda,\xi)}_{\mathbf{k}}\right)-\rho_0\left(\mathcal{E}^{(\lambda',\xi)}_{\mathbf{k}'}\right)}{\left(\mathcal{E}^{(\lambda,\xi)}_{\mathbf{k}}-\mathcal{E}^{(\lambda',\xi)}_{\mathbf{k}'}\right)}\right]$$
$$\times\ \langle\Psi_{\mathbf{k},\lambda}||\hat{j}_\alpha(\mathbf{R})||\Psi_{\mathbf{k}',\lambda'}|\rangle|\langle\Psi_{\mathbf{k}',\lambda'}||\hat{j}_\beta(\mathbf{R}')||\Psi_{\mathbf{k},\lambda}\rangle. \tag{C25}$$

Note that the first term in the numerator of the first square bracket

$$\frac{-i\left(\mathcal{E}^{(\lambda,\xi)}_{\mathbf{k}}-\mathcal{E}^{(\lambda',\xi)}_{\mathbf{k}'}\right)}{\left(\mathcal{E}^{(\lambda,\xi)}_{\mathbf{k}}-\mathcal{E}^{(\lambda',\xi)}_{\mathbf{k}'}\right)^2+\hbar^2s^2}\left[\frac{\rho_0\left(\mathcal{E}^{(\lambda,\xi)}_{\mathbf{k}}\right)-\rho_0\left(\mathcal{E}^{(\lambda',\xi)}_{\mathbf{k}'}\right)}{\left(\mathcal{E}^{(\lambda,\xi)}_{\mathbf{k}}-\mathcal{E}^{(\lambda',\xi)}_{\mathbf{k}'}\right)}\right] = -i\frac{\rho_0\left(\mathcal{E}^{(\lambda,\xi)}_{\mathbf{k}}\right)-\rho_0\left(\mathcal{E}^{(\lambda',\xi)}_{\mathbf{k}'}\right)}{\left(\mathcal{E}^{(\lambda,\xi)}_{\mathbf{k}}-\mathcal{E}^{(\lambda',\xi)}_{\mathbf{k}'}\right)^2+\hbar^2s^2} \tag{C26}$$

is odd in the integration variables, and therefore, has zero contribution. As expected, no imaginary part survives. For the real part, we use

$$\lim_{s\to0^+}\frac{\hbar s}{\left(\mathcal{E}^{(\lambda,\xi)}_{\mathbf{k}}-\mathcal{E}^{(\lambda',\xi)}_{\mathbf{k}'}\right)^2+\hbar^2s^2} = \pi\delta\left(\mathcal{E}^{(\lambda,\xi)}_{\mathbf{k}}-\mathcal{E}^{(\lambda',\xi)}_{\mathbf{k}'}\right), \tag{C27}$$

so that for the term in the second square bracket

$$\left[\frac{\rho_0\left(\mathcal{E}^{(\lambda,\xi)}_{\mathbf{k}}\right)-\rho_0\left(\mathcal{E}^{(\lambda',\xi)}_{\mathbf{k}'}\right)}{\left(\mathcal{E}^{(\lambda,\xi)}_{\mathbf{k}}-\mathcal{E}^{(\lambda',\xi)}_{\mathbf{k}'}\right)}\right]\delta\left(\mathcal{E}^{(\lambda,\xi)}_{\mathbf{k}}-\mathcal{E}^{(\lambda',\xi)}_{\mathbf{k}'}\right)$$
$$= \left.\frac{\partial f_0(E)}{\partial E}\right|_{E=\mathcal{E}^{(\lambda,\xi)}_{\mathbf{k}}}\delta(\mathcal{E}^{(\lambda,\xi)}_{\mathbf{k}}-\mathcal{E}^{(\lambda',\xi)}_{\mathbf{k}'}), \tag{C28}$$

where $f_0(E,T) = (1+\exp[(E-\mu)/k_BT])^{-1}$ is the Fermi-Dirac distribution. Then

$$L^{(11)}_{\alpha\beta}(\mathbf{R},\mathbf{R}')$$
$$= -\pi\hbar v_F^2T\sum_{\lambda,\lambda'}\int\frac{d^2k}{(2\pi)^2}\int\frac{d^2k'}{(2\pi)^2}\left.\frac{\partial f_0(E)}{\partial E}\right|_{E=\mathcal{E}^{(\lambda,\xi)}_{\mathbf{k}}}$$
$$\times\ \delta\left(\mathcal{E}^{(\lambda,\xi)}_{\mathbf{k}}-\mathcal{E}^{(\lambda',\xi)}_{\mathbf{k}'}\right)$$
$$\times\ \Psi^\dagger_{\mathbf{k},\lambda}(\mathbf{R})\sigma_\alpha\Psi_{\mathbf{k}',\lambda'}(\mathbf{R})\Psi^\dagger_{\mathbf{k}',\lambda'}(\mathbf{R}')\sigma_\beta\Psi_{\mathbf{k},\lambda}(\mathbf{R}'), \tag{C29}$$

where we have used the representation of the current operator in Eq. (C20). On the other hand, we know that

$$\Psi^\dagger_{\mathbf{k},\lambda}(\mathbf{R})\sigma_\alpha\Psi_{\mathbf{k}',\lambda'}(\mathbf{R})\Psi^\dagger_{\mathbf{k}',\lambda'}(\mathbf{R}')\sigma_\beta\Psi_{\mathbf{k},\lambda}(\mathbf{R}')$$
$$= \mathrm{Tr}[\sigma_\alpha\Psi_{\mathbf{k}',\lambda'}(\mathbf{R})\otimes\Psi^\dagger_{\mathbf{k}',\lambda'}(\mathbf{R}')\sigma_\beta\Psi_{\mathbf{k},\lambda}(\mathbf{R}')\otimes\Psi^\dagger_{\mathbf{k},\lambda}(\mathbf{R})], \tag{C30}$$

and by defining the spectral function $\mathcal{A}^\xi(\mathbf{R},\mathbf{R}';E)$:

$$\mathcal{A}^\xi(\mathbf{R},\mathbf{R}';E)$$
$$= 2\pi\sum_\lambda\int\frac{d^2k}{(2\pi)^2}\Psi_{\mathbf{k},\lambda}(\mathbf{R})\otimes\Psi^\dagger_{\mathbf{k},\lambda}(\mathbf{R}')\delta\left(E-\mathcal{E}^{(\lambda,\xi)}_{\mathbf{k}}\right), \tag{C31}$$

together with the identity

$$\int\frac{d^3k}{(2\pi)^3}\sum_\lambda g\left(\mathcal{E}^{(\lambda,\xi)}_{\mathbf{k}}\right)\Psi_{\mathbf{k},\lambda}(\mathbf{R})\otimes\Psi^\dagger_{\mathbf{k},\lambda}(\mathbf{R}')$$
$$= \int_{-\infty}^{\infty}\frac{dE}{2\pi}\mathcal{A}^\xi(\mathbf{R},\mathbf{R}';E)g(E), \tag{C32}$$

we arrive at the result

$$L^{(11)}_{\alpha\beta}(\mathbf{R},\mathbf{R}') = -\frac{\hbar v_F^2T}{2\pi}\int_{-\infty}^{\infty}dE\ \frac{\partial f_0(E)}{\partial E}$$
$$\times\ \mathrm{Tr}[\sigma_\alpha\mathcal{A}^\xi(\mathbf{R},\mathbf{R}';E)\sigma_\beta\mathcal{A}^\xi(\mathbf{R}',\mathbf{R};E)], \tag{C33}$$

where an additional factor of 2 comes from the spin degeneracy.

The other Onsager's coefficients are obtained by the same fashion, so that:

$$L^{(12)}_{\alpha\beta}(\mathbf{R},\mathbf{R}') = L^{(21)}_{\alpha\beta}(\mathbf{R},\mathbf{R}')$$
$$= -\frac{\hbar v_F^2T}{2\pi}\int_{-\infty}^{\infty}dE\ \frac{\partial f_0(E)}{\partial E}(E-\mu)$$
$$\times\ \mathrm{Tr}[\sigma_\alpha\mathcal{A}^\xi(\mathbf{R},\mathbf{R}';E)\sigma_\beta\mathcal{A}^\xi(\mathbf{R}',\mathbf{R};E)], \tag{C34}$$

and

$$L^{(22)}_{\alpha\beta}(\mathbf{R},\mathbf{R}') = -\frac{\hbar v_F^2T}{2\pi}\int_{-\infty}^{\infty}dE\ \frac{\partial f_0(E)}{\partial E}(E-\mu)^2$$
$$\times\ \mathrm{Tr}[\sigma_\alpha\mathcal{A}^\xi(\mathbf{R},\mathbf{R}';E)\sigma_\beta\mathcal{A}^\xi(\mathbf{R}',\mathbf{R};E)]. \tag{C35}$$

Let us work on the spectral function. Its coordinate representation is given by

$$\mathcal{A}^\xi(\mathbf{R},\mathbf{R}';E)$$
$$= \int\frac{d^2k}{(2\pi)^2}e^{i\mathbf{k}\cdot(\mathbf{R}-\mathbf{R}')}\sum_\lambda\left(\sigma_0+\lambda\frac{\boldsymbol{\sigma}\cdot\mathbf{k}}{|\mathbf{k}|}\right)\mathcal{A}^{(\lambda,\xi)}(k;E), \tag{C36}$$

so that by inserting Eqs. (C33)–(C35) we have

$$L^{(11)}_{\alpha\beta}(\mathbf{R},\mathbf{R}') = \int\frac{d^2q}{(2\pi)^2}e^{i\mathbf{q}\cdot(\mathbf{R}-\mathbf{R}')}$$
$$\times\left(\frac{\hbar v_F^2T}{2\pi}\right)\int_{-\infty}^{\infty}dE\left(-\frac{\partial f_0(E)}{\partial E}\right)$$
$$\times\int\frac{d^2k}{(2\pi)^2}\mathrm{Tr}[\sigma_\alpha\mathcal{A}^\xi(\mathbf{k}+\mathbf{q};E)\sigma_\beta\mathcal{A}^\xi(\mathbf{k};E)]$$
$$= \int\frac{d^2q}{(2\pi)^2}e^{i\mathbf{q}\cdot(\mathbf{R}-\mathbf{R}')}L^{(11)}_{\alpha\beta}(\mathbf{q};T). \tag{C37}$$

Without loss of generality, we will define the Onsager's coefficients in the limit $\mathbf{q} \to 0$. Then:

$$L^{(11)}_{\alpha\beta}(T) = \lim_{\mathbf{q}\to 0} L^{(11)}_{\alpha\beta}(\mathbf{q};T) = \left(\frac{\hbar v_F^2 T}{2\pi}\right)\int_{-\infty}^{\infty} dE\left(-\frac{\partial f_0(E)}{\partial E}\right) \times \int \frac{d^2k}{(2\pi)^2}\mathcal{A}^{(\lambda,\xi)}(k;E)\mathcal{A}^{(\lambda,\xi)}(k;E) \times \mathrm{Tr}\left[\sigma_\alpha\left(\sigma_0 + \lambda\frac{\boldsymbol{\sigma}\cdot\mathbf{k}}{k}\right)\sigma_\beta\left(\sigma_0 + \lambda\frac{\boldsymbol{\sigma}\cdot\mathbf{k}}{k}\right)\right]. \tag{C38}$$

From the $SU(2)$ algebra, we can readily obtain the trace

$$\mathrm{Tr}\left[\sigma_\alpha\left(\sigma_0 + \lambda\frac{\boldsymbol{\sigma}\cdot\mathbf{k}}{k}\right)\sigma_\beta\left(\sigma_0 + \lambda\frac{\boldsymbol{\sigma}\cdot\mathbf{k}}{k}\right)\right] = 4\frac{k_\alpha k_\beta}{k^2}, \tag{C39}$$

and hence we have

$$L^{(11)}_{\alpha\beta}(T) = 4\left(\frac{\hbar v_F^2 T}{2\pi}\right)\int_{-\infty}^{\infty} dE\left(-\frac{\partial f_0(E)}{\partial E}\right) \times \int \frac{d^2k}{(2\pi)^2}\frac{k_\alpha k_\beta}{k^2}\mathcal{A}^{(\lambda,\xi)}(k;E)\mathcal{A}^{(\lambda,\xi)}(k;E). \tag{C40}$$

Performing the angular integral over polar coordinates $d^2k = d\phi dk k$ first, we get

$$\int \frac{d^2k}{(2\pi)^2}\frac{k_\alpha k_\beta}{k^2} = \frac{\delta_{\alpha\beta}}{(2\pi)^2}\frac{\pi}{2}\int_0^\infty dk\frac{\mathbf{k}\cdot\mathbf{k}}{k}. \tag{C41}$$

Finally, using the definition of the spectral function in terms of the retarded and advanced disorder-averaged Green's functions,

$$\mathcal{A}^{(\lambda,\xi)}(k;E) = i\left[\left\langle G_R^{(\lambda,\xi)}(k;E)\right\rangle - \left\langle G_A^{(\lambda,\xi)}(k;E)\right\rangle\right], \tag{C42}$$

we obtain (in the limit of low impurity concentrations $n_{\mathrm{imp}} \ll 1$)

$$L^{(11)}_{\alpha\beta}(T) = \delta_{\alpha\beta}4\pi\left(\frac{\hbar v_F^2 T}{(2\pi)^3}\right)\int_{-\infty}^{\infty} dE\left(-\frac{\partial f_0(E)}{\partial E}\right) \times \int_0^\infty dk\left\langle G_R^{(\lambda,\xi)}(k;E)\right\rangle\left\langle G_A^{(\lambda,\xi)}(k;E)\right\rangle\frac{\mathbf{k}\cdot\mathbf{k}}{k}. \tag{C43}$$

### 3. The vertex corrections and relaxation time

To include the vertex corrections, as described in Ref. [12], we can formally perform the substitution $\mathbf{k} \to \boldsymbol{\Gamma}_{\mathrm{RA}}(\mathbf{k};E)$ for one of the momenta in the integral. Here, $\boldsymbol{\Gamma}_{\mathrm{RA}}(\mathbf{k};E)$ is the solution to the *Bethe-Salpeter equation* depicted in the diagram Fig. 4, given by

$$\boldsymbol{\Gamma}_{\mathrm{RA}}(\mathbf{k},E) = \mathbf{k} + n_{\mathrm{imp}}\int \frac{d^2k'}{(2\pi)^2}\left\langle G_R^{(\lambda,\xi)}(\mathbf{k}')\right\rangle\left\langle G_A^{(\lambda,\xi)}(\mathbf{k}')\right\rangle \times \left|\hat{T}^{(\lambda,\xi)}_{\mathbf{k}'\mathbf{k}}\right|^2\boldsymbol{\Gamma}_{\mathrm{RA}}(\mathbf{k}',E). \tag{C44}$$

where $\hat{T}^{(\lambda,\xi)}_{\mathbf{k}'\mathbf{k}}$ is the $T$-matrix operator.

Hence, we have

$$L^{(11)}_{\alpha\beta}(T) = \delta_{\alpha\beta}\frac{\hbar v_F^2 T}{2\pi^2}\int_{-\infty}^{\infty} dE\left(-\frac{\partial f_0(E)}{\partial E}\right) \times \int_0^\infty dk\left\langle G_R^{(\lambda,\xi)}(\mathbf{k})\right\rangle\left\langle G_A^{(\lambda,\xi)}(\mathbf{k})\right\rangle\frac{\mathbf{k}\cdot\boldsymbol{\Gamma}_{\mathrm{RA}}(\mathbf{k},E)}{k}, \tag{C45}$$

$$L^{(12)}_{\alpha\beta}(T) = \delta_{\alpha\beta}\frac{\hbar v_F^2 T}{2\pi^2}\int_{-\infty}^{\infty} dE\left(-\frac{\partial f_0(E)}{\partial E}\right)(E-\mu) \times \int_0^\infty dk\left\langle G_R^{(\lambda,\xi)}(\mathbf{k})\right\rangle\left\langle G_A^{(\lambda,\xi)}(\mathbf{k})\right\rangle\frac{\mathbf{k}\cdot\boldsymbol{\Gamma}_{\mathrm{RA}}(\mathbf{k},E)}{k}, \tag{C46}$$

and

$$L^{(22)}_{\alpha\beta}(T) = \delta_{\alpha\beta}\frac{\hbar v_F^2 T}{2\pi^2}\int_{-\infty}^{\infty} dE\left(-\frac{\partial f_0(E)}{\partial E}\right)(E-\mu)^2 \times \int_0^\infty dk\left\langle G_R^{(\lambda,\xi)}(\mathbf{k})\right\rangle\left\langle G_A^{(\lambda,\xi)}(\mathbf{k})\right\rangle\frac{\mathbf{k}\cdot\boldsymbol{\Gamma}_{\mathrm{RA}}(\mathbf{k},E)}{k}. \tag{C47}$$

Now, the vertex function must be of the form $\boldsymbol{\Gamma}_{\mathrm{RA}}(\mathbf{k},E) = \gamma(\mathbf{k},E)\mathbf{k}$, with $\gamma(\mathbf{k},E)$ a scalar function. Moreover, in the limit of low impurity concentration $n_{\mathrm{imp}} \ll 1$ we have

$$\left\langle G_R^{(\lambda,\xi)}(\mathbf{k})\right\rangle\left\langle G_A^{(\lambda,\xi)}(\mathbf{k})\right\rangle \to \frac{2\pi\tau(k)}{\hbar}\delta(E - \lambda\xi\hbar v_F k). \tag{C48}$$

Then, in such a limit, we obtain a secular integral equation for the scalar function $\gamma(\mathbf{k},E)$

$$\gamma(\mathbf{k},E) = 1 + n_{\mathrm{imp}}\frac{2\pi}{\hbar}\int\frac{d^2k'}{(2\pi)^2}\tau(k') \times \left|T^{(\lambda,\xi)}_{\mathbf{k}'\mathbf{k}}\right|^2\delta(E - \lambda\xi\hbar v_F k')\ \gamma(\mathbf{k}',E)\frac{\mathbf{k}\cdot\mathbf{k}'}{k^2}. \tag{C49}$$

At low temperatures, an exact solution is possible since the derivative of the Fermi distribution takes a compact support at the Fermi energy. Therefore, we can evaluate $\gamma(k;E)$ and $\tau(k)$ at the Fermi momentum $k_F$, to obtain

$$\gamma(k_F) = \frac{\tau_1(k_F)}{\tau_1(k_F) - \tau(k_F)}, \tag{C50}$$

where we defined (for $\cos\phi' = \mathbf{k}\cdot\mathbf{k}'/k^2$)

$$\frac{1}{\tau_1(k_F)} = \frac{2\pi n_{\mathrm{imp}}}{\hbar}\int\frac{d^2k'}{(2\pi)^2}\left|T^{(\lambda,\xi)}_{\mathbf{k}'\mathbf{k}}\right|^2\cos\phi'\ \delta(\hbar v_F k_F - \hbar v_F k'). \tag{C51}$$

After the substitution of $\gamma(\mathbf{k},E)$ from Eq. (C50), and the simple relation

$$-\frac{\partial f_0(E)}{\partial E} = \frac{1}{k_B T}f_0(E)[1 - f_0(E)] \tag{C52}$$

we finally obtain for the bulk Onsager coefficients

$$L^{(11)}_{\alpha\alpha}(T) = \frac{v_F^2}{\pi k_B}\tau_{\mathrm{tr}}(k_F)\int_0^\infty dk k\, f_0\left(\mathcal{E}^{(\lambda,\xi)}_{\mathbf{k}}\right)\left[1 - f_0\left(\mathcal{E}^{(\lambda,\xi)}_{\mathbf{k}}\right)\right], \tag{C53}$$

$$L_{\alpha\alpha}^{(12)}(T)=\frac{v_F^2}{\pi k_B}\tau_{\rm tr}(k_F)\int_0^\infty dk k\, f_0\big(\mathcal{E}_{\mathbf{k}}^{(\lambda,\xi)}\big)\big[1-f_0\big(\mathcal{E}_{\mathbf{k}}^{(\lambda,\xi)}\big)\big]\times(\lambda\xi\hbar v_F k-\mu), \tag{C54}$$

and

$$L_{\alpha\alpha}^{(22)}(T)=\frac{v_F^2}{\pi k_B}\tau_{\rm tr}(k_F)\times\int_0^\infty dk\, k\, f_0\big(\mathcal{E}_{\mathbf{k}}^{(\lambda,\xi)}\big)\big[1-f_0\big(\mathcal{E}_{\mathbf{k}}^{(\lambda,\xi)}\big)\big]\times(\lambda\xi\hbar v_F k-\mu)^2. \tag{C55}$$

By following Ref. [12] the total *transport relaxation time* is defined by

$$\frac{1}{\tau_{\rm tr}(k_F)}=\frac{1}{\tau(k_F)}-\frac{1}{\tau_1(k_F)}=\frac{2\pi n_{\rm imp}}{\hbar}\int\frac{d^2k'}{(2\pi)^2}\delta(\hbar v_F k_F-\hbar v_F k')\big|T_{\mathbf{k}'\mathbf{k}}^{(\lambda,\xi)}\big|^2\times(1-\cos\phi'), \tag{C56}$$

which can be expressed in terms of the scattering phase shifts $\delta_m(k)$

$$\frac{1}{\tau_{\rm tr}(k_F)}=\frac{2n_{\rm imp}v_F}{k_F}\sum_{m=-\infty}^{\infty}\sin^2\left[\delta_m(k_F)-\delta_{m-1}(k_F)\right]. \tag{C57}$$

#### 4. The electrical conductivity

Note that $f_0(\varepsilon)[1-f_0(\varepsilon)]=f_0(\varepsilon)f_0(-\varepsilon)$ is an even function of its argument. Then we can write

$$f_0\big(\mathcal{E}_{\mathbf{k}}^{(\lambda,\xi)}\big)\big[1-f_0\big(\mathcal{E}_{\mathbf{k}}^{(\lambda,\xi)}\big)\big]=\frac{e^{\lambda\xi(\hbar v_F k-\lambda\xi\mu)/k_BT}}{(e^{\lambda\xi(\hbar v_F k-\lambda\xi\mu)/k_BT}+1)^2}=\frac{e^{(\hbar v_F k-\lambda\xi\mu)/k_BT}}{(e^{(\hbar v_F k-\lambda\xi\mu)/k_BT}+1)^2}, \tag{C58}$$

provided by the fact that $\lambda\xi=\pm1$. Let us introduce the variables

$$x=\frac{\hbar v_F}{k_BT}k,\quad \tilde{\mu}=\frac{\lambda\xi\mu}{k_BT}, \tag{C59}$$

so that

$$f_0(x)[1-f_0(x)]=\frac{e^{x-\tilde{\mu}}}{(e^{x-\tilde{\mu}}+1)^2}=\frac{\partial}{\partial\tilde{\mu}}\left(\frac{1}{e^{x-\tilde{\mu}}+1}\right). \tag{C60}$$

This change of variables implies that the desired integrals have the form

$$I_n=\frac{d}{d\tilde{\mu}}\int_0^\infty\frac{x^n}{e^{x-\tilde{\mu}}+1}dx,\quad \text{for } n=2,3,4. \tag{C61}$$

By using the integral representation of the Polylogarithm function

$$-\mathrm{Li}_s(-z)=\frac{1}{\Gamma(s)}\int_0^\infty\frac{x^{s-1}}{e^x/z+1}dx, \tag{C62}$$

and the derivative relation

$$\frac{d}{d\tilde{\mu}}\mathrm{Li}_s(-e^{\tilde{\mu}})=\mathrm{Li}_{s-1}(-e^{\tilde{\mu}}), \tag{C63}$$

one can show that the integral of interest is

$$I_n=-n!\,\mathrm{Li}_n(-e^{\tilde{\mu}}). \tag{C64}$$

Thus,

$$L_{\alpha\alpha}^{(11)(\lambda,\xi)}(T)=\frac{v_F^2}{\pi k_B}\tau_{\rm tr}(k_F)\int_0^\infty dk\,k\,f_0\big(\mathcal{E}_{\mathbf{k}}^{(\lambda,\xi)}\big)\big[1-f_0\big(\mathcal{E}_{\mathbf{k}}^{(\lambda,\xi)}\big)\big]=\frac{v_F^2}{\pi k_B}\tau_{\rm tr}(k_F)\left(\frac{k_BT}{\hbar v_F}\right)^2\frac{d}{d\tilde{\mu}}\int_0^\infty\frac{x}{e^{x-\tilde{\mu}}+1}dx=\frac{1}{\pi k_B}\left(\frac{k_BT}{\hbar}\right)^2\tau_{\rm tr}(k_F)\,I_1, \tag{C65}$$

or by defining the chemical potential as $\mu=\hbar v_F k_F$

$$L_{\alpha\alpha}^{(11)(\lambda,\xi)}(T)=\frac{1}{\pi k_B}\left(\frac{k_BT}{\hbar}\right)^2\tau_{\rm tr}(k_F)\ln\left(1+e^{\frac{\lambda\xi\hbar v_F k_F}{k_BT}}\right). \tag{C66}$$

The electrical conductivity is then obtained from Eq. (C8)

$$\sigma_{\alpha\beta}=\frac{e^2}{T}\sum_{\lambda=\pm1}\sum_{\xi=\pm1}L_{\alpha\alpha}^{(11)(\lambda,\xi)}(T)=\frac{2e^2}{T}\frac{1}{\pi k_B}\left(\frac{k_BT}{\hbar}\right)^2\tau_{\rm tr}(k_F)\times\left[\ln\left(1+e^{\frac{\hbar v_F k_F}{k_BT}}\right)+\ln\left(1+e^{\frac{-\hbar v_F k_F}{k_BT}}\right)\right]=\frac{2e^2k_BT}{\pi\hbar^2}\tau_{\rm tr}(k_F)\left[\ln\left(e^{\frac{\hbar v_F k_F}{k_BT}}\right)+2\ln\left(1+e^{-\frac{\hbar v_F k_F}{k_BT}}\right)\right], \tag{C67}$$

which after some elementary algebra reduces to Eq. (57).

#### 5. The thermal conductivity and Seebeck coefficient

By following the same procedure, the other coefficients are

$$L_{\alpha\alpha}^{(12)(\lambda,\xi)}(T)=\lambda\xi\frac{v_F^2}{\pi k_B}\tau_{\rm tr}(k_F)\times\int_0^\infty dk\,k\,f_0\big(\mathcal{E}_{\mathbf{k}}^{(\lambda,\xi)}\big)\big[1-f_0\big(\mathcal{E}_{\mathbf{k}}^{(\lambda,\xi)}\big)\big](\hbar v_F k-\tilde{\mu}\cdot k_BT)=\lambda\xi\frac{v_F^2}{\pi k_B}\tau_{\rm tr}(k_F)\left(\frac{k_BT}{\hbar v_F}\right)^2(k_BT)\times\left[\frac{d}{d\tilde{\mu}}\int_0^\infty\frac{x^2}{e^{x-\tilde{\mu}}+1}dx-\tilde{\mu}\frac{d}{d\tilde{\mu}}\int_0^\infty\frac{x}{e^{x-\tilde{\mu}}+1}dx\right]=\frac{\lambda\xi}{\pi}\frac{\hbar}{k_B}\left(\frac{k_BT}{\hbar}\right)^3\tau_{\rm tr}(k_F)[I_2-\tilde{\mu}I_1], \tag{C68}$$

and

$$L_{\alpha\alpha}^{(22)(\lambda,\xi)}(T)=\frac{v_F^2}{\pi k_B}\tau_{\rm tr}(k_F)\times\int_0^\infty dk\,k\,f_0\big(\mathcal{E}_{\mathbf{k}}^{(\lambda,\xi)}\big)\big[1-f_0\big(\mathcal{E}_{\mathbf{k}}^{(\lambda,\xi)}\big)\big](\hbar v_F k-\tilde{\mu}\cdot k_BT)^2$$

$$= \frac{v_F^2}{\pi k_B}\tau_{\rm tr}(k_F)\left(\frac{k_BT}{\hbar v_F}\right)^2 (k_BT)^2 \times\left[\frac{d}{d\tilde{\mu}}\int_0^\infty \frac{x^3}{e^{x-\tilde{\mu}}+1}dx - 2\tilde{\mu}\frac{d}{d\tilde{\mu}}\int_0^\infty \frac{x^2}{e^{x-\tilde{\mu}}+1}dx + \tilde{\mu}^2\frac{d}{d\tilde{\mu}}\int_0^\infty \frac{x}{e^{x-\tilde{\mu}}+1}dx\right]$$
$$= \frac{\hbar^2}{\pi k_B}\left(\frac{k_BT}{\hbar}\right)^4 \tau_{\rm tr}(k_F)[I_3 - 2\tilde{\mu}\, I_2 + \tilde{\mu}^2\, I_1], \tag{C69}$$

so that

$$L_{\alpha\alpha}^{(12)(\lambda,\xi)}(T) = -\frac{2\lambda\xi}{\pi}\frac{\hbar}{k_B}\left(\frac{k_BT}{\hbar}\right)^3\tau_{\rm tr}(k_F) \times\left[\mathrm{Li}_2\left(-e^{\frac{\lambda\xi\hbar v_F k_F}{k_BT}}\right) - \frac{\lambda\xi\hbar v_F k_F}{k_BT}\mathrm{Li}_1\left(-e^{\frac{\lambda\xi\hbar v_F k_F}{k_BT}}\right)\right], \tag{C70}$$

and

$$L_{\alpha\alpha}^{(22)(\lambda,\xi)}(T) = -\frac{2\hbar^2}{\pi k_B}\left(\frac{k_BT}{\hbar}\right)^4\tau_{\rm tr}(k_F) \times\left[3\,\mathrm{Li}_3\left(-e^{\frac{\lambda\xi\hbar v_F k_F}{k_BT}}\right) - 2\lambda\xi\frac{\hbar v_F k_F}{k_BT}\mathrm{Li}_2\left(-e^{\frac{\lambda\xi\hbar v_F k_F}{k_BT}}\right) + \frac{1}{2}\left(\frac{\hbar v_F k_F}{k_BT}\right)^2\mathrm{Li}_1\left(-e^{\frac{\lambda\xi\hbar v_F k_F}{k_BT}}\right)\right]. \tag{C71}$$

Then, the thermal conductivity is obtained by replacing Eqs. (C65), (C68), and (C69) into Eq. (C12)

$$\kappa_{\alpha\alpha}^{(\lambda\xi)}(T) = \frac{1}{T^2}\left[L_{\alpha\alpha}^{(22)(\lambda,\xi)}(T) - \frac{L_{\alpha\alpha}^{(12)(\lambda,\xi)}(T)L_{\alpha\alpha}^{(21)(\lambda,\xi)}(T)}{L_{\alpha\alpha}^{(11)(\lambda,\xi)}(T)}\right] = \frac{\hbar^2}{\pi k_BT^2}\left(\frac{k_BT}{\hbar}\right)^4\tau_{\rm tr}(k_F)\left(I_3 - \frac{I_2^2}{I_1}\right), \tag{C72}$$

in such a way that the final result is

$$\kappa_{\alpha\alpha}(T) = -\frac{2\hbar^2}{\pi k_BT^2}\left(\frac{k_BT}{\hbar}\right)^4\tau_{\rm tr}(k_F) \times\sum_{\lambda,\xi=\pm1}\left[3\,\mathrm{Li}_3\left(-e^{\frac{\lambda\xi\hbar v_F k_F}{k_BT}}\right) - 2\frac{\left[\mathrm{Li}_2\left(-e^{\frac{\lambda\xi\hbar v_F k_F}{k_BT}}\right)\right]^2}{\ln\left(1+e^{\frac{\lambda\xi\hbar v_F k_F}{k_BT}}\right)}\right]. \tag{C73}$$

The Seebeck coefficient is obtained replacing Eqs. (C65) and (C68) into Eq. (C13)

$$S(T) = \frac{1}{eT}\sum_{(\lambda,\xi)}\frac{L_{\alpha\alpha}^{(12)(\lambda,\xi)}(T)}{L_{\alpha\alpha}^{(11)(\lambda,\xi)}(T)} = -\frac{k_B}{e}\sum_{\lambda=\pm1}\sum_{\xi=\pm1}\left(\frac{2\lambda\xi\,\mathrm{Li}_2\left(-e^{\frac{\lambda\xi\hbar v_F k_F}{k_BT}}\right)}{\ln\left(1+e^{\frac{\lambda\xi\hbar v_F k_F}{k_BT}}\right)} + \frac{\hbar v_F k_F}{k_BT}\right). \tag{C74}$$


[1] Aristotle, Book VIII, *Metaphysics* (Clarendon Press, New York, 1999), pp. 1045a.8–10.

[2] A. K. Geim and I. V. Grigorieva, Van der waals heterostructures, Nature **499**, 419 (2013).

[3] C.-K. Chiu, J. C. Y. Teo, A. P. Schnyder, and S. Ryu, Classification of topological quantum matter with symmetries, Rev. Mod. Phys. **88**, 035005 (2016).

[4] M. Z. Hasan and C. L. Kane, Colloquium: Topological insulators, Rev. Mod. Phys. **82**, 3045 (2010).

[5] M. Z. Hasan, S.-Y. Xu, I. Belopolski, and S.-M. Huang, Discovery of weyl fermion semimetals and topological fermi arc states, Annu. Rev. Condens. Matter Phys. **8**, 289 (2017).

[6] P. Roushan, J. Seo, C. V. Parker, Y. S. Hor, D. Hsieh, D. Qian, A. Richardella, M. Z. Hasan, R. J. Cava, and A. Yazdani, Topological surface states protected from backscattering by chiral spin texture, Nature **460**, 1106 (2009).

[7] N. Xu, Y. Xu, and J. Zhu, Topological insulators for thermoelectrics, npj Quant. Mater. **2**, 51 (2017).

[8] X.-L. Qi, T. L. Hughes, and S.-C. Zhang, Topological field theory of time-reversal invariant insulators, Phys. Rev. B **78**, 195424 (2008).

[9] M. Fiebig, Revival of the magnetoelectric effect, J. Phys. D: Appl. Phys. **38**, R123 (2005).

[10] J. D. Castaño-Yepes, O. J. Franca, C. F. Ramirez-Gutierrez, and J. C. del Valle, Optical intersubband properties of a core-shell semiconductor-topological insulator quantum dot described by $\theta$-electrodynamics, Phys. E **123**, 114202 (2020).

[11] J. D. Castaño-Yepes, D. J. Nader, and A. Martín-Ruiz, Ground state andpolarization of an hydrogen-like atom near a Weyl semimetal, Phys. Rev. A **107**, 032814 (2023).

[12] D. Bonilla and E. Muñoz, Electronic transport in Weyl semimetals with a uniform concentration of torsional dislocations, Nanomaterials **12**, 3711 (2022).

[13] H. Falomir, M. Loewe, and E. Muñoz, Chemical sensing with graphene: A quantum field theory perspective, Phys. Rev. B **103**, 235431 (2021).

[14] V. Juričić, E. Muñoz, and R. Soto-Garrido, Optical conductivity as a probe of the interaction-driven metal in rhombohedral trilayer graphene, Nanomaterials **12**, 3727 (2022).

[15] J. Zhang, C.-Z. Chang, P. Tang, Z. Zhang, X. Feng, K. Li, L. li Wang, X. Chen, C. Liu, W. Duan, K. He, Q.-K. Xue, X. Ma, and Y. Wang, Topology-driven magnetic quantum phase transition in topological insulators, Science **339**, 1582 (2013).

[16] J. Maciejko, X.-L. Qi, H. D. Drew, and S.-C. Zhang, Topological Quantization in Units of the Fine Structure Constant, Phys. Rev. Lett. **105**, 166803 (2010).

[17] A. Martín-Ruiz, M. Cambiaso, and L. F. Urrutia, Green's function approach to Chern-Simons extended electrodynamics: An effective theory describing topological insulators, Phys. Rev. D **92**, 125015 (2015).

[18] A. Martín-Ruiz, M. Cambiaso, and L. F. Urrutia, Electro- and magnetostatics of topological insulators as modeled by planar,

spherical, and cylindrical $\theta$ boundaries: Green's function approach, Phys. Rev. D **93**, 045022 (2016).
[19] A. Martín-Ruiz, M. Cambiaso, and L. F. Urrutia, Electromagnetic description of three-dimensional time-reversal invariant ponderable topological insulators, Phys. Rev. D **94**, 085019 (2016).
[20] A. Martín-Ruiz, Magnetoelectric effect in cylindrical topological insulators, Phys. Rev. D **98**, 056012 (2018).
[21] X.-L. Qi, R. Li, J. Zang, and S.-C. Zhang, Inducing a magnetic monopole with topological surface states, Science **323**, 1184 (2009).
[22] S. Das Sarma, S. Adam, E. H. Hwang, and E. Rossi, Electronic transport in two-dimensional graphene, Rev. Mod. Phys. **83**, 407 (2011).
[23] E. Muñoz, Phonon-limited transport coefficients in extrinsic graphene, J. Phys.: Condens. Matter **24**, 195302 (2012).
[24] G. D. Mahan, *Many-Particle Physics* (Kluwer Academic/Plenum, New York, 2000).
[25] O. J. Franca and S. Y. Buhmann, Modification of transition radiation by three-dimensional topological insulators, Phys. Rev. B **105**, 155120 (2022).
[26] O. J. Franca and L. F. Urrutia, Radiation from a dipole perpendicular to the interface between two planar semi-infinite magnetoelectric media, Rev. Mex. Fis **68**, 060701 (2021).
[27] A. De Martino and R. Egger, Two-electron bound states near a coulomb impurity in gapped graphene, Phys. Rev. B **95**, 085418 (2017).
[28] T. O. Wehling, M. I. Katsnelson, and A. I. Lichtenstein, Impurities on graphene: Midgap states and migration barriers, Phys. Rev. B **80**, 085428 (2009).
[29] Z. M. Gibbs, A. LaLonde, and G. J. Snyder, Optical band gap and the Burstein–Moss effect in iodine doped PbTe using diffuse reflectance infrared Fourier transform spectroscopy, New J. Phys. **15**, 075020 (2013).
[30] A. D. LaLonde, Y. Pei, and G. J. Snyder, Reevaluation of $PbTe_{1-x}I_x$ as high performance n-type thermoelectric material, Energy Environ. Sci. **4**, 2090 (2011).
[31] D. L. Greenaway and G. Harbeke, Band structure of bismuth telluride, bismuth selenide and their respective alloys, J. Phys. Chem. Solids **26**, 1585 (1965).
[32] I. T. Witting, T. C. Chasapis, F. Ricci, M. Peters, N. A. Heinz, G. Hautier, and G. J. Snyder, The thermoelectric properties of bismuth telluride, Adv. Electron. Mater. **5**, 1800904 (2019).
[33] H. Wang, J. Wang, X. Cao, and G. J. Snyder, Thermoelectric alloys between pbse and pbs with effective thermal conductivity reduction and high figure of merit, J. Mater. Chem. A **2**, 3169 (2014).
[34] H. Wang, Y. Pei, A. D. LaLonde, and G. J. Snyder, Weak electron?phonon coupling contributing to high thermoelectric performance in n-type PbSe, Proc. Natl. Acad. Sci. USA **109**, 9705 (2012).
[35] H. Wang, Y. Pei, A. D. LaLonde, and G. Jeffery Snyder, Material design considerations based on thermoelectric quality factor, in *Thermoelectric Nanomaterials* (Springer, Berlin, 2013), pp. 3–32.
[36] C.-Y. Lee, Relativistic corrections to the semiconducting properties of selected materials, Phys. Rev. B **35**, 4511 (1987).
[37] Y. Xia, D. Qian, D. Hsieh, L. Wray, A. Pal, H. Lin, A. Bansil, D. Grauer, Y. S. Hor, R. J. Cava *et al.*, Observation of a large-gap topological-insulator class with a single Dirac cone on the surface, Nat. Phys. **5**, 398 (2009).
[38] O. Madelung, U. Rössler, and M. Schulz, Group IV elements, IV–IV and III–V compounds: Part B—Electronic, transport, optical and other properties, in *Semiconductors* (Springer, Berlin, 2002).
[39] J. Bardeen and W. Shockley, Deformation potentials and mobilities in non-polar crystals, Phys. Rev. **80**, 72 (1950).
[40] I. Strzalkowski, S. Joshi, and C. R. Crowell, Dielectric constant and its temperature dependence for GaAs, CdTe, and ZnSe, Appl. Phys. Lett. **28**, 350 (1976).
[41] J. O. Akinlami and A. O. Ashamu, Optical properties of GaAs, J. Semicond. **34**, 032002 (2013).
[42] D. L. Rode, Electron Transport in InSb, InAs, and InP, Phys. Rev. B **3**, 3287 (1971).
[43] K. M. Demchuk and I. M. Tsidilkovskii, Scattering of electrons by the deformation potential in doped InSb, Phys. Status Solidi (b) **82**, 59 (1977).
[44] E. Muñoz and R. Soto-Garrido, Analytic approach to magneto-strain tuning of electronic transport through a graphene nanobubble: Perspectives for a strain sensor, J. Phys.: Condens. Matter **29**, 445302 (2017).
[45] R. Soto-Garrido, E. Muñoz, and V. Juričić, Dislocation defect as a bulk probe of monopole charge of multi-weyl semimetals, Phys. Rev. Res. **2**, 012043(R) (2020).
[46] D. Bonilla, E. Muñoz, and R. Soto-Garrido, Thermo-magneto-electric transport through a torsion dislocation in a type i weyl semimetal, Nanomaterials **11**, 2972 (2021).
[47] E. Muñoz and R. Soto-Garrido, Thermoelectric transport in torsional strained weyl semimetals, J. Appl. Phys. **125**, 082507 (2019).
[48] N. N. Lebedev and R. A. Silverman, *Special Functions and Their Applications*, Dover Books on Mathematics (Dover, Mineola, NY, 1972).